Research article

JGS
Journal of the Geological Society

https://doi.org/10.1144/jgs2022-067 | Vol. 180 | 2022 | jgs2022-067

# Cretaceous magmatism in the Antarctic Peninsula and its tectonic implications

**Joaquin Bastias[1,2,3]*, Richard Spikings[1], Teal Riley[4], David Chew[2], Anne Grunow[5], Alexey Ulianov[6], Massimo Chiaradia[1] and Alex Burton-Johnson[4]**

[1] Department of Earth Sciences, University of Geneva, 1205 Genève, Switzerland
[2] Department of Geology, Trinity College Dublin, College Green, Dublin 2, Ireland
[3] Carrera Geología, Facultad de Ingeniería, Universidad Andres Bello, Santiago, Chile
[4] British Antarctic Survey, High Cross, Madingley Road, Cambridge CB3 0ET, UK
[5] Byrd Polar Research Center, Ohio State University, 108 Scott Hall, 1090 Carmack Road, Columbus, OH 43210, USA
[6] Institute of Earth Sciences, University of Lausanne, 1015 Lausanne, Switzerland
JB, 0000-0001-6678-3173
* Correspondence: joaquin.bastias@unige.ch

**Abstract:** Periods of cessation, resumption and enhanced arc activity are recorded in the Cretaceous igneous rocks of the Antarctic Peninsula. We present new geochronological (laser ablation inductively coupled plasma mass spectrometry (LA-ICP-MS) zircon U–Pb) analyses of 36 intrusive and volcanic Cretaceous rocks, along with LA-ICP-MS apatite U–Pb analyses (a medium-temperature thermochronometer) of 28 Triassic–Cretaceous igneous rocks of the Antarctic Peninsula. These are complemented by new zircon Hf isotope data along with whole-rock geochemistry and isotope (Nd, Sr and Pb) data. Our results indicate that the Cretaceous igneous rocks of the Antarctic Peninsula have geochemical signatures consistent with a continental arc setting and were formed during the interval *c.* 140–79 Ma, whereas the main peak of magmatism occurred during *c.* 118–110 Ma. Trends in $\varepsilon Hf_t$ (zircon) combined with elevated heat flow that remagnetized rocks and reset apatite U–Pb ages suggest that Cretaceous magmatism formed within a prevailing extensional setting that was punctuated by periods of compression. A noteworthy compressive period probably occurred during *c.* 147–128 Ma, triggered by the westward migration of South America during opening of the South Atlantic Ocean. Cretaceous arc rocks that crystallized during *c.* 140–100 Ma define a belt that extends from southeastern Palmer Land to the west coast of Graham Land. This geographical distribution could be explained by (1) a flat slab with east-dipping subduction of the Phoenix Plate, or (2) west-dipping subduction of the lithosphere of the Weddell Sea, or (3) an allochthonous origin for the rocks of Alexander Island. A better understanding of the geological history of the pre-Cretaceous rocks of Alexander Island and the inaccessible area of the southern Weddell Sea is required.

**Supplementary material:** A description of the methods used in this study and the complete dataset are available at https://doi.org/10.6084/m9.figshare.c.6089274

**Received** 4 May 2022; **revised** 6 July 2022; **accepted** 7 July 2022

The Antarctic Peninsula hosts one of the major Mesozoic–Cenozoic continental magmatic arcs of the circum-Pacific, which extends almost continuously for *c.* 1350 km along the length of the peninsula (Pankhurst 1982; Leat *et al.* 1995; Millar *et al.* 2002). Arc rocks were emplaced from the Late Triassic (Leat *et al.* 1995; Bastias *et al.* 2020) to the Miocene (e.g. Leat *et al.* 1995; Jordan *et al.* 2014), with a surge in magmatic volume during the Cretaceous (Leat *et al.* 1995; Riley *et al.* 2018; Jordan *et al.* 2020). These arc-related rocks intrude late Paleozoic–Triassic sedimentary sequences in Graham Land (e.g. Pankhurst 1983; Castillo *et al.* 2016) and Triassic metamorphic orthogneisses (Millar *et al.* 2002; Flowerdew *et al.* 2006) associated with an active margin in Palmer Land (Bastias *et al.* 2020; Riley *et al.* 2020*b*).

Globally, Cretaceous arc magmatism is considered to represent a significant Phanerozoic phase of growth of the continental crust (e.g. Kemp *et al.* 2009; Ducea *et al.* 2015). Regionally, the Cretaceous is also characterized by significant deformation along much of the western margin of Gondwana (e.g. Vaughan and Livermore 2005; Bryan and Ferrari 2013), which was accompanied by a global plate reorganization event (Matthews *et al.* 2012). Arc magmatism along the Antarctic Peninsula formed during east-dipping subduction of Pacific oceanic lithosphere beneath the Antarctic plate in southwestern Gondwana (Fig. 1a; e.g. Pankhurst 1990; Burton-Johnson and Riley 2015; Bastias *et al.* 2021*a*). Evidence of arc magmatism includes individual plutons, composite intrusions and extensive batholith-like units (e.g. Leat *et al.* 1995). Previous studies of the Cretaceous peak of arc magmatism in the Antarctic Peninsula have focused on their episodicity (Riley *et al.* 2018) and magmatic–tectonic relationships (Burton-Johnson *et al.* in press), although the regional processes that controlled and triggered a higher rate of magma addition to the crust remain unclear.

The aim of this study is to further constrain the magmatic and tectonic evolution of the Cretaceous arc of the Antarctic Peninsula by providing new geochronological, geochemical and isotopic data, and integrating our data with the timing of magmatism, subduction architecture and tectonic history presented in previous studies. We present 36 new zircon U–Pb (crystallization) dates (obtained using laser ablation inductively coupled plasma mass spectrometry; LA-ICP-MS), and geochemical (whole-rock) and isotopic (whole-rock Nd, Sr, Pb; zircon Hf) data acquired from Cretaceous igneous units exposed in the Antarctic Peninsula (Graham and Palmer Land; Fig. 1b). These are complemented by mid-temperature (>350°C) apatite U–Pb thermochronology data obtained by LA-ICP-MS. The igneous rocks crop out in remote locations that were sampled during two field seasons as part of this study, or samples were provided by the British Antarctic Survey archive and the Byrd Polar and Climate Research Center, USA. We combine our data with previous results

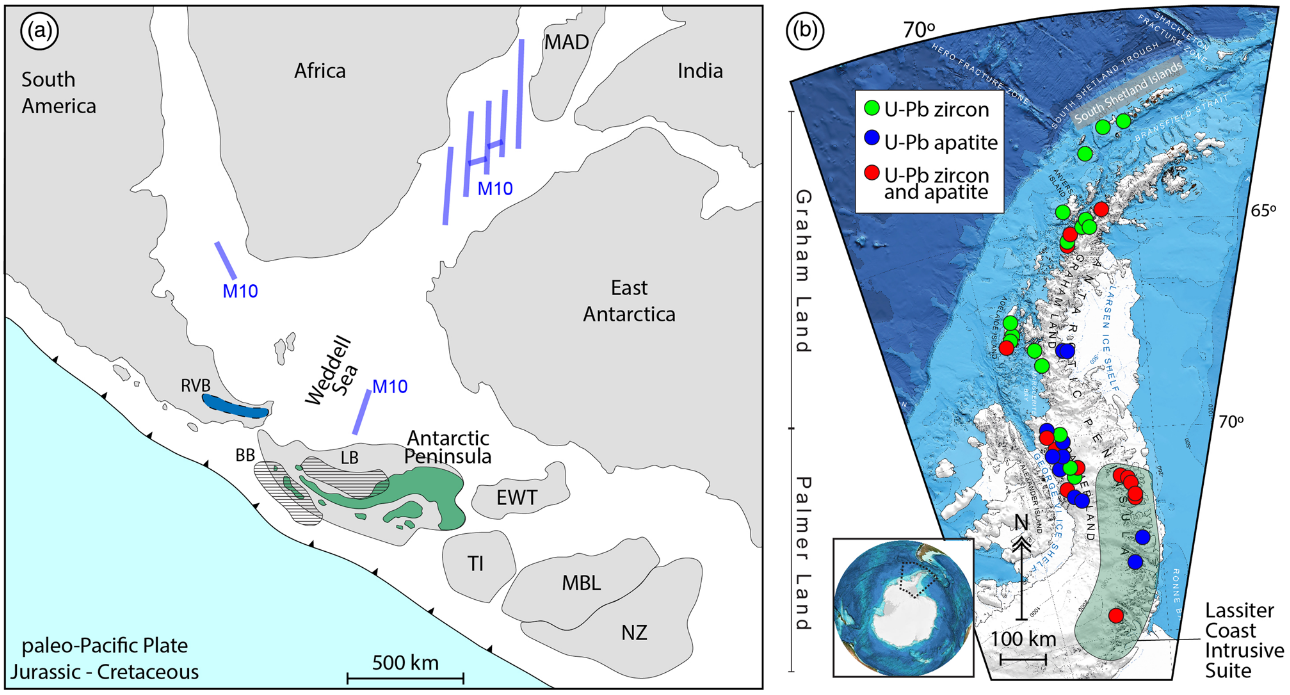


**Fig. 1.** (**a**) Palaeogeographical reconstruction of the Pacific active margin of Gondwana during the Jurassic–Cretaceous (e.g. Ghidella *et al.* 2002; Jokat *et al.* 2003; Martin 2007), showing the Antarctic Peninsula crustal block in green. BB, Byers Basin (Bastias *et al.* 2019); EWT, Ellsworth Whitmore Mountains, Larsen Basin (LB) (Hathway 2000); MAD, Madagascar; MBL, Marie Byrd Land; M10, *c.* 134 Ma (e.g. Martin 2007); NZ, New Zealand; RVB, Rocas Verdes Basin (e.g. Calderón *et al.* 2007); TI, Thurston Island. (**b**) Present-day map of the Antarctic Peninsula showing the location of the studied rocks. These samples were either collected in the field during the 2015 and 2016 Antarctic campaign of the Instituto Antártico Chileno (INACH) or provided by the British Antarctic Survey and the Polar Rock Repository at Ohio State University. Sample locations are presented along with the dating method: green, U–Pb LA-ICP-MS zircon; blue, U–Pb LA-ICP-MS apatite; red, combined U–Pb LA-ICP-MS zircon and apatite.

from the Antarctic Peninsula (Riley *et al.* 2001, 2016, 2018, 2020*a*; Ryan 2007; Leat *et al.* 2009; Haase *et al.* 2012; Bastias 2014, 2020; Bastias *et al.* 2019, 2020, 2021*a*, *b*; Burton-Johnson et al. in press).

## Geological framework and previous work

The continental crust of the Antarctic Peninsula was interpreted by Suárez (1976) to represent an autochthonous segment of an extensive continental arc that spanned Mesozoic western Gondwana. Alternatively, other researchers have suggested that the Antarctic Peninsula crust formed by collision and accretion of an allochthonous arc with a block of Gondwanan affinity either during the middle of the Cretaceous (Vaughan and Storey 2000) or earlier, close to the Jurassic–Triassic boundary (Vaughan *et al.* 2012). More recently, Burton-Johnson and Riley (2015) and Bastias *et al.* (2020) provided substantial geochronological and isotopic evidence for an autochthonous to parautochthonous Mesozoic evolution, with subduction initiation during the Late Paleozoic, supporting the initial interpretation of Suárez (1976).

Arc magmatism along the Antarctic Peninsula occurred from at least the Late Triassic (Pankhurst 1982; Bastias *et al.* 2020; Riley *et al.* 2020*b*), when it formed a segment of the Terra Australis margin of western Gondwana (e.g. Cawood 2005). Subsequently, a Late Triassic active margin was associated with the Rymill Granite Complex (Bastias *et al.* 2020), which is mostly composed of orthogneisses and is widely exposed in the central Antarctic Peninsula and formed during an extensional tectonic regime that modified the entire Pacific margin of west Gondwana (Spikings *et al.* 2016). Early Jurassic arc magmatism was concentrated in Palmer Land (Riley *et al.* 2017; Bastias *et al.* 2021*a*) and shifted to Graham Land during the Middle–Late Jurassic (e.g. Bastias *et al.* 2021*a*). Most of the Jurassic magmatic rocks in the Antarctic Peninsula have been linked to the influence of an active margin and perhaps the migration of the Karoo mantle plume from southern Africa as well (Pankhurst *et al.* 2000; Riley *et al.* 2001). However, Bastias *et al.* (2021*a*) recently suggested that most Jurassic magmatism probably formed within an active margin that was characterized by a flat-slab setting.

Cretaceous magmatic rocks are exposed along the west coast of Graham Land and in eastern Palmer Land (Fig. 2a). Magma addition rates to the Antarctic Peninsula peaked during the Early Cretaceous (e.g. Leat *et al.* 1995, 2009; Riley *et al.* 2018), which is considered to be the most voluminous episode of Phanerozoic plutonism in the Antarctic Peninsula (e.g. Leat *et al.* 1995, 2009; Vaughan *et al.* 2012; Riley *et al.* 2018; Burton-Johnson *et al.* in press). These rocks range from mafic to felsic compositions, but are predominantly intermediate, and the published radiometric dates (K–Ar, Rb–Sr, $^{40}Ar/^{39}Ar$ and U–Pb methods) range between *c.* 141 and *c.* 67 Ma (Leat *et al.* 1995).

Early Cretaceous volcanic rocks are abundant along the west coast of the Antarctic Peninsula and the South Shetland Islands (Fig. 2a; e.g. Leat *et al.* 1995). Most of these are basalts and andesites with a calc-alkaline affinity (e.g. Haase *et al.* 2012). The Early Cretaceous plutonic record includes a few exposures on the South Shetland Islands (*c.* 137–109 Ma; Hervé *et al.* 2006; Bastias *et al.* 2019) and in SE Palmer Land, where the Lassiter Coast Intrusive Suite is exposed (Fig. 2a; Rowley *et al.* 1983; Riley *et al.* 2018; Burton-Johnson *et al.* in press). These rocks are mainly tonalite, quartz diorite and granodiorite and crop out over an area of *c.* 80 000 km$^2$ (Fig. 2a; Burton-Johnson *et al.* in press). Zircon U–Pb concordia dates suggest that the Lassiter Coast Intrusive Suite was emplaced in three pulses at 130–126, 118–113 and 108–102 Ma (Riley *et al.* 2018). Burton-Johnson *et al.* (in press) further resolved the central episode of magmatism with secondary pulses at *c.* 118–116, *c.* 114–112 and *c.* 110–109 Ma, which are consistent with the model of Paterson and Ducea (2015).

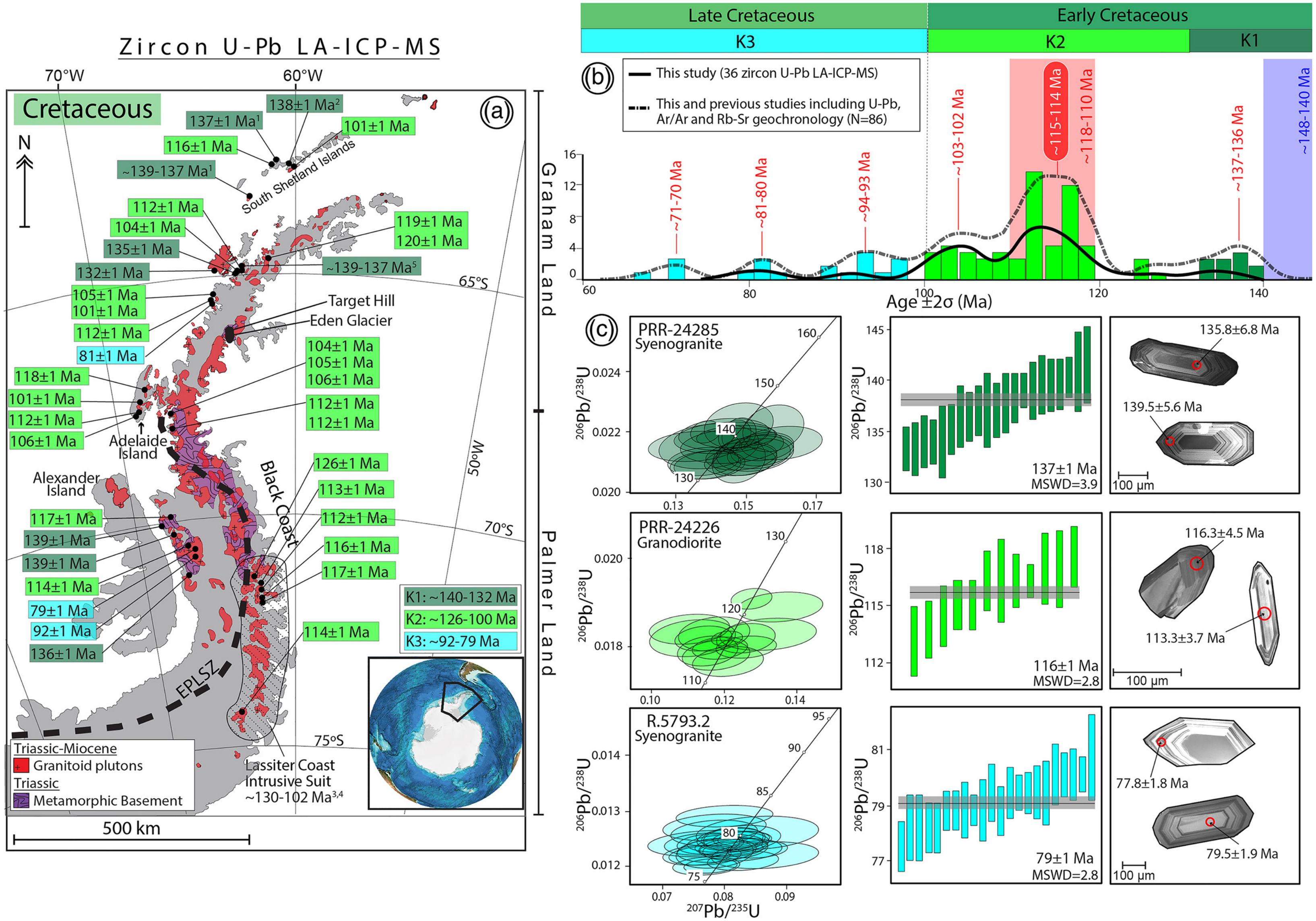


**Fig. 2.** (**a**) Geological map of the Antarctic Peninsula, showing the distribution of intrusive rocks (red) and the Rymill Granite Complex (purple), modified from Burton-Johnson and Riley (2015). Zircon $^{206}Pb/^{238}U$ concordia (LA-ICP-MS) and $^{40}Ar/^{39}Ar$ plateau ages collected in this study are shown along with published, pre-Jurassic U/Pb ages and correspond to: [1]Bastias *et al.* (2019); [2]Hervé *et al.* (2006); [3]Riley *et al.* (2018); [4]Burton-Johnson *et al.* (in press); [5]Ryan (2007). All uncertainties are quoted at ±2σ. Three periods are outlined, *c.* 140–132 Ma (dark green), *c.* 126–100 Ma (light green) and *c.* 92–79 Ma (turquoise). EPLSZ, Eastern Palmer Land Shear Zone, from Vaughan and Storey (2000) and Vaughan *et al.* (2012). (**b**) Kernel density estimates of the distribution of crystallization ages during the Cretaceous (black line, this study; dot–dash line, this and previous work). An age peak occurs at *c.* 118–110 Ma (main peak at *c.* 115–114 Ma) with minor peaks at *c.* 137–136, *c.* 103–102, *c.* 94–93, *c.* 81–80 and *c.* 71–70 Ma (all in red). Magmatic quiescence is recorded at *c.* 148–140 Ma (in blue). (**c**) Representative Wetherill concordia plots of zircon U–Pb data obtained from the Cretaceous igneous rocks of the Antarctic Peninsula. Bars represent single ablation spots and represent an uncertainty of 2σ. Representative cathodoluminescence (SEM) images of the dated zircons are presented.

Pankhurst *et al.* (1991) and Leat *et al.* (2009) obtained whole-rock $^{87}Sr/^{86}Sr_i$ and $\varepsilon Nd_i$ values from the Early Cretaceous volcanic rocks of the Antarctic Peninsula, which span 0.7080–0.7056 and −0.4 to −1.8, respectively, from rocks that yielded Rb–Sr ages of *c.* 132–116 Ma.

Late Cretaceous igneous rocks are less widely exposed (Fig. 2a; e.g. Leat *et al.* 1995), with isolated calc-alkaline granodioritic plutons associated with Late Cretaceous mafic dykes in the central Antarctic Peninsula (Wever *et al.* 1994; Leat *et al.* 1995). Most of the mafic dykes yield calc-alkaline compositions, although some ocean island basalt-like mafic dykes occur locally (Leat and Riley 2021), which Leat *et al.* (1995) utilized to infer an extensional setting. Ryan (2007) obtained zircon LA-ICP-MS U–Pb concordia dates that range between *c.* 92 and 89 Ma, and $^{87}Sr/^{86}Sr_i$ and $\varepsilon Nd_i$ values that span 0.7047–0.7045 and 2.5–2.2, respectively, for plutons exposed in west–central Graham Land (Fig. 2a). Leat *et al.* (2009) reported Rb–Sr isochron ages between *c.* 96 and *c.* 71 Ma for volcanic rocks located within the central–western Antarctic Peninsula, which yield whole-rock $^{87}Sr/^{86}Sr_i$ and $\varepsilon Nd_i$ values of 0.7112–0.7056, and 0.0 to −1.8, respectively. Recently, Riley *et al.* (2020*a*) published U–Pb zircon dates ranging between *c.* 94 and 64 Ma from felsic volcanic rocks located in northwestern and central Palmer Land and suggested that arc magmatism migrated trenchward during the Late Cretaceous along the southern Antarctic Peninsula, which is consistent with previous work (e.g. Thomson and Pankhurst 1983; Leat *et al.* 1995). In contrast, the locus of magmatism in Graham Land does not appear to change with respect to the trench throughout the Cretaceous.

An extensional regime dominated the Antarctic Peninsula during the Cretaceous, as evidenced by the emplacement of large volumes of magmatic rocks as plutons and dykes, accompanied by normal faults (Meneilly *et al.* 1987; Wever *et al.* 1994; Leat *et al.* 1995). However, the Cretaceous period was also associated with brief compressional events at *c.* 138, *c.* 113 and *c.* 107–100 Ma in the Antarctic Peninsula (e.g. Meneilly 1988; Leat *et al.* 1995; Vaughan and Storey 2000; Riley *et al.* 2020*a*). These compressional events have been linked either to increases in the subduction convergence rate (at *c.* 138 and *c.* 113 Ma; e.g. Riley *et al.* 2020*a*) or to the collision of an allochthonous terrane (*c.* 107–100 Ma Vaughan and Storey 2000). The latter collisional event has been disputed in more recent studies (Burton-Johnson and Riley 2015; Bastias *et al.* 2020). A more extensive compressional episode along western Gondwana has been proposed (e.g. Vaughan 1995; Mpodozis *et al.* 2005; Vaughan and Livermore 2005; Burton-Johnson and Riley 2015; Spikings *et al.* 2015; Boyce *et al.* 2020).

## Methods

We present new zircon U–Pb geochronological, geochemical and isotopic data from 36 igneous rocks of the Antarctic Peninsula (Fig. 1). The rocks were taken from the Lassiter Coast Intrusive Suite in eastern Palmer Land, and from intrusions that are scattered along the west coast of central Palmer Land at the latitude of the Black Coast. Additional plutonic rocks were collected from the west coast of Graham Land and the South Shetland Islands. The methods used in this work are described in detail in the Supplementary material.

## Results

### *Zircon LA-ICP-MS U–Pb geochronology*

We present U–Pb zircon concordia ages from 36 igneous rocks that vary in age between 139 ± 1 and 79 ± 1 Ma (Table 1; Fig. 2a). Early Cretaceous ages were obtained from 33 samples, and range from 139 ± 1 to 101 ± 1 Ma, with no particular geographical trend (Fig. 2a). Three samples yield Late Cretaceous ages from 92 ± 1 to 79 ± 1 Ma and are located along the west coast of the Antarctic Peninsula. The kernel density estimate (KDE) of the $^{206}Pb/^{238}U$ concordia ages yields several peaks during the Cretaceous, and these have been separated into three groups to facilitate the presentation of the data. These groups are (1) a cluster of older ages at *c.* 140–132 Ma (Berriasian–Valanginian–Hauterivian), (2) a younger group that includes several KDE peaks from 126 to 100 Ma (Barremian–Albian) and (3) the youngest group with Late Cretaceous ages spanning *c.* 92–79 Ma (Turonian–Campanian; using the International Chronostratigraphic Chart time scale of Cohen *et al.* 2013; Fig. 2b). Cathodoluminescence images (see examples in Fig. 2c) show that most zircons have patchy or oscillatory zonation, mostly with no clear rim–core relationships; all are typical of igneous zircon (e.g. Chelle-Michou *et al.* 2014).

Six granodiorites and monzogranites of the Lassiter Coast Intrusive Suite yield $^{206}Pb/^{238}U$ concordia dates of *c.* 126–112 Ma (Fig. 2a), consistent with previous studies (*c.* 130–102 Ma; Pankhurst *et al.* 1991; Riley *et al.* 2018; Burton-Johnson *et al.* in press). Further north, seven samples from the west coast of Palmer Land yield zircon $^{206}Pb/^{238}U$ concordia dates of *c.* 140–79 Ma (Fig. 2a), whereas five monzogranites, syenogranites, tonalites and quartz-monzonites are Early Cretaceous in age (*c.* 139–114 Ma) and two syenogranites have Late Cretaceous ages (92 ± 1 and 79 ± 1 Ma). At the latitude of Adelaide Island (*c.* 67°S), eight alkali granites, granodiorites and quartz-monzonites yield Early Cretaceous dates that span *c.* 118–101 Ma (Fig. 2a). Further north, seven alkali granites, syenogranites, monzogranites and monzodiorites from the west coast of southern Graham Land also yield Early Cretaceous ages that span *c.* 135–101 Ma, whereas a gabbro yields a Late Cretaceous date of 81 ± 1 Ma (Fig. 2a). The northernmost Cretaceous $^{206}Pb/^{238}U$ concordia dates were obtained from three monzogranites and a granodiorite from the South Shetland Islands, which span *c.* 138–101 Ma, and are consistent with previous age estimates of volcanic and intrusive rocks from that region (Hervé *et al.* 2006; Bastias 2014; Israel 2015; Bastias *et al.* 2019). These data show that Early Cretaceous rocks occur extensively along the Antarctic Peninsula from the SE in Palmer Land to the NW in Graham Land, whereas Late Cretaceous plutons are less abundant, and crop out along the west coast of the central and northern Antarctic Peninsula (Fig. 2a). The complete dataset is presented in Supplementary material Table 1.

### *Apatite LA-ICP-MS U–Pb thermochronology*

Apatite U–Pb LA-ICP-MS dates have been obtained from the Cretaceous rocks that were used for U–Pb zircon LA-ICP-MS geochronology in this study, and also from Late Triassic (Bastias *et al.* 2020) and Jurassic igneous rocks (Bastias *et al.* 2021*a*; Table 2; Fig. 3) previously dated by the U–Pb zircon LA-ICP-MS method. For each sample, single spot analyses are plotted in Tera–Wasserburg space where they represent a mixture of radiogenic ($^{206}Pb$) and initial (common) lead ($^{207}Pb/^{206}Pb$). In the case of rapid cooling and no subsequent perturbation of the U–Pb system, a sample containing a suite of cogenetic crystals with a large spread in radiogenic Pb/common Pb ratios (Fig. 4) can be used to define a well-constrained linear array in Tera–Wasserburg space (e.g. Kirkland *et al.* 2018). However, this assumes U–Pb concordance in the sample (e.g. Petrus and Kamber 2012) and requires a significant spread in the radiogenic Pb/common Pb ratios to ensure a well-constrained linear array (Kirkland *et al.* 2018). Linear regressions through the data from each sample yield 28 $^{238}U/^{206}Pb$ (Tera–Wasserburg concordia lower intercept) dates that range between 147 ± 15 and 76 ± 25 Ma, whereas the

**Table 1.** *Summary of the geochronological and isotopic tracing data collected from the Cretaceous igneous rocks in the Antarctic Peninsula presented in this work*

| | | | | | | Whole-rock isotopic tracing | | | | |
|---|---|---|---|---|---|---|---|---|---|---|
| Sample | South | West | Age (Ma) | Error | MSWD | $^{87}Sr/^{86}Sr_i$ | $\varepsilon Nd_i$ | $^{206}Pb/^{204}Pb_i$ | $^{207}Pb/^{204}Pb_i$ | $^{208}Pb/^{204}Pb_i$ |
| R5297.1 | −70.63 | −67.15 | 139 | 1 | 6.3 | 0.7062 | −0.4 | 18.67 | 15.66 | 38.57 |
| R6057.3 | −70.39 | −67.92 | 139 | 1 | 1.6 | 0.7046 | 4.1 | 18.57 | 15.63 | 38.38 |
| PRR-24285 | −63.22 | −62.25 | 137 | 1 | 3.9 | 0.7053 | 2.3 | 18.82 | 15.65 | 38.68 |
| PRR-24201 | −63.22 | −62.25 | 137 | 1 | 4.5 | | | | | |
| R6317.1 | −71.51 | −67.12 | 136 | 1 | 3.3 | 0.7080 | −4.9 | 18.76 | 15.66 | 38.59 |
| PRR-5985 | −64.90 | −63.05 | 135 | 1 | 4.7 | | | | | |
| 15JB45 | −64.77 | −64.09 | 132 | 1 | 0.6 | 0.7040 | | 18.51 | 15.61 | 38.36 |
| N11.142.1 | −71.42 | −63.58 | 126 | 1 | 2.0 | 0.7056 | −0.8 | 19.00 | 15.67 | 38.57 |
| PRR-5991 | −64.57 | −61.55 | 120 | 1 | 4.4 | | | | | |
| PRR-5990 | −64.57 | −61.55 | 119 | 1 | 4.8 | 0.7090 | −0.3 | 18.83 | 15.66 | 38.66 |
| J6.386.1 | −67.27 | −68.19 | 118 | 1 | 10.9 | | | | | |
| R5939.2 | −70.22 | −66.68 | 117 | 1 | 0.9 | 0.7060 | −2.1 | 18.62 | 15.65 | 38.46 |
| N11.15.1 | −71.72 | −62.57 | 117 | 1 | 2.2 | 0.7053 | −0.8 | 18.62 | 15.64 | 38.06 |
| PRR-24226 | −62.73 | −61.20 | 116 | 1 | 2.8 | 0.7049 | 1.9 | 18.63 | 15.64 | 38.48 |
| N11.12.1 | −71.73 | −62.52 | 116 | 1 | 1.9 | | | | | |
| R5979.1 | −70.93 | −66.26 | 115 | 1 | 2.7 | 0.7068 | −2.6 | 18.78 | 15.66 | 38.60 |
| P14.03.1 | −74.32 | −64.63 | 114 | 1 | 3.5 | 0.7053 | −2.7 | 18.85 | 15.65 | 38.67 |
| N11.8.1 | −71.50 | −63.01 | 113 | 1 | 3.2 | 0.7100 | −9.7 | 18.73 | 15.66 | 38.47 |
| N11.3.1 | −71.56 | −62.82 | 112 | 1 | 1.6 | 0.7057 | −3.1 | 18.80 | 15.66 | 38.62 |
| J6.290.1 | −67.60 | −68.74 | 112 | 1 | 2.5 | 0.7050 | −0.9 | 18.65 | 15.64 | 38.52 |
| PRR-6061 | −64.88 | −62.55 | 112 | 1 | 1.7 | 0.7054 | −0.2 | 18.93 | 15.66 | 38.60 |
| PRR-6031 | −65.25 | −64.08 | 112 | 1 | 1.7 | 0.7041 | 0.9 | 18.84 | 15.65 | 38.71 |
| PRR-5992 | −68.13 | −67.12 | 112 | 1 | 2.4 | 0.7061 | −5.7 | 18.31 | 15.63 | 38.45 |
| PRR-5994 | −68.13 | −67.12 | 112 | 1 | 2.9 | | | | | |
| 15JB53 | −64.83 | −62.86 | 104 | 1 | 1.3 | 0.7050 | 0.7 | 18.70 | 15.64 | 38.55 |
| PRR-6000 | −67.82 | −67.18 | 106 | 1 | 3.3 | 0.7052 | −0.4 | 18.80 | 15.65 | 38.60 |
| J6.297.1 | −67.63 | −68.75 | 106 | 1 | 1.7 | 0.7052 | 0.6 | 18.70 | 15.64 | 38.55 |
| PRR-6023 | −65.20 | −64.10 | 105 | 1 | 2.1 | | | | | |
| PRR-5999 | −67.82 | −67.18 | 105 | 1 | 2.4 | | | | | |
| PRR-5998 | −67.82 | −67.18 | 105 | 1 | 1.3 | | | | | |
| PRR-32819 | −62.72 | −60.37 | 101 | 1 | 2.8 | | | | | |
| PRR-6025 | −65.20 | −64.10 | 101 | 1 | 2.4 | 0.7049 | 1.3 | 18.63 | 15.63 | 38.47 |
| J6.307.1 | −67.47 | −68.53 | 101 | 1 | 8.3 | | | | | |
| R5905.4 | −71.28 | −66.13 | 92 | 1 | 1.8 | 0.7060 | −0.8 | 18.78 | 15.65 | 38.60 |
| PRR-6034 | −65.28 | −64.10 | 81 | 1 | 1.0 | 0.7044 | −1.3 | 18.38 | 15.60 | 38.36 |
| R5793.2 | −70.94 | −66.80 | 79 | 1 | 2.8 | 0.7068 | −1.9 | 18.82 | 15.66 | 38.65 |

All the ages were obtained by zircon LA-ICP-MS U–Pb analysis.

**Table 2.** *Summary of the U–Pb apatite and zircon data for the Triassic–Cretaceous rocks of the Antarctic Peninsula*

| | | | | | Apatite | | | | | Zircon–$^{206}Pb/^{238}U$ | | |
|---|---|---|---|---|---|---|---|---|---|---|---|---|
| | | | | | $^{206}Pb/^{238}U$ (lower intercept) | | | $^{206}Pb/^{238}U$ (higher intercept) | | | | |
| Sample | Internal code | South | West | Source | Age | 2σ | MSWD | Intercept | 2σ | U–Pb zircon | 2σ | MSWD |
| 18JB26 | R5957.3 | −70.70 | −67.57 | Bastias *et al.* (2021*a*, *b*) | 139 | 11 | 9.3 | 0.8710 | 0.063 | 156 | 1 | 1.2 |
| 18JB34 | K7.526.3 | −68.20 | −65.18 | Bastias *et al.* (2020) | 145 | 13 | 3.2 | 0.7350 | 0.051 | 215 | 2 | 1.1 |
| 18JB43 | K7.562 | −68.19 | −65.30 | Bastias *et al.* (2020) | 135 | 10 | 3.0 | 0.8270 | 0.014 | 218 | 1 | 1.1 |
| 18JB50 | R.6307.1 | −71.58 | −66.89 | Bastias *et al.* (2021*a*, *b*) | 142 | 7 | 2.3 | 0.8190 | 0.017 | 153 | 1 | 1.3 |
| 15JB76 | PRR-5990 | −64.57 | −61.55 | This study | 113 | 10 | 1.8 | 0.8256 | 0.011 | 119 | 1 | 4.8 |
| 18JB32 | R5257.5 | −70.03 | −67.65 | Bastias *et al.* (2021*a*, *b*) | 143 | 6 | 1.8 | 0.8259 | 0.008 | 183 | 1 | 1.1 |
| 18JB27 | R.5290.1 | −70.53 | −66.80 | Bastias *et al.* (2020) | 131 | 6 | 1.7 | 0.8321 | 0.006 | 216 | 2 | 1.6 |
| N14-35 | | −72.75 | −61.33 | Burton-Johnson *et al.* in press | 119 | 7 | 1.7 | 0.8267 | 0.020 | 117 | 2 | 0.2 |
| 18JB31 | R5297.1 | −70.63 | −67.15 | This study | 134 | 5 | 1.6 | 0.8220 | 0.030 | 139 | 1 | 6.3 |
| 18JB14 | N11.12.1 | −71.73 | −62.52 | This study | 120 | 4 | 1.5 | 0.8297 | 0.010 | 116 | 1 | 1.9 |
| 15JB79 | PRR-6034 | −65.28 | −64.10 | This study | 76 | 25 | 1.4 | 0.8232 | 0.016 | 81 | 1 | 1.0 |
| 18JB02 | R.6067.8 | −70.69 | −66.58 | Bastias *et al.* (2020) | 128 | 26 | 1.4 | 0.8316 | 0.009 | 208 | 3 | 1.1 |
| 18JB08 | N11.142.1 | −71.42 | −63.58 | This study | 135 | 4 | 1.4 | 0.8378 | 0.019 | 126 | 1 | 2.0 |
| 18JB18 | R.6306.7 | −71.61 | −66.35 | Bastias *et al.* (2020) | 135 | 10 | 1.4 | 0.8335 | 0.013 | 212 | 2 | 1.3 |
| 18JB20 | R.5786.3 | −70.92 | −66.92 | Bastias *et al.* (2020) | 147 | 15 | 1.4 | 0.8295 | 0.008 | 203 | 1 | 1.0 |
| 18JB28 | J6.297.1 | −67.63 | −68.75 | This study | 123 | 10 | 1.4 | 0.8515 | 0.008 | 106 | 1 | 1.7 |
| 18JB30 | R6317.1 | −71.51 | −67.12 | This study | 145 | 4 | 1.4 | 0.8350 | 0.009 | 136 | 1 | 3.3 |
| N14-57 | | −73.30 | −62.40 | Burton-Johnson *et al.* in press | 115 | 5 | 1.4 | 0.8209 | 0.017 | 117 | 1 | 0.5 |
| N15-139 | | −73.30 | −62.40 | Burton-Johnson *et al.* in press | 117 | 8 | 1.4 | 0.8279 | 0.013 | 118 | 1 | 0.7 |
| 16JB63 | PRR-6025 | −65.20 | −64.10 | This study | 93 | 51 | 1.3 | 0.8250 | 0.025 | 101 | 1 | 2.4 |
| 18JB06 | N11.8.1 | −71.50 | −63.01 | This study | 118 | 5 | 1.3 | 0.8310 | 0.010 | 113 | 1 | 3.2 |
| 18JB15 | N11.15.1 | −71.72 | −62.57 | This study | 118 | 4 | 1.2 | 0.8183 | 0.013 | 117 | 1 | 2.2 |
| 18JB36 | R6057.3 | −70.39 | −67.92 | This study | 142 | 5 | 1.2 | 0.8000 | 0.026 | 139 | 1 | 1.6 |
| 16JB62 | PRR-6023 | −65.20 | −64.10 | This study | 109 | 19 | 1.1 | 0.8370 | 0.033 | 105 | 1 | 2.1 |
| 18JB21 | R5979.1 | −70.93 | −66.26 | This study | 102 | 15 | 1.1 | 0.8170 | 0.015 | 115 | 1 | 2.7 |
| 18JB67 | P14.03.1 | −74.32 | −64.63 | This study | 126 | 11 | 1.0 | 0.8292 | 0.017 | 114 | 1 | 3.45 |
| 15JB77 | PRR-5991 | −64.57 | −61.55 | This study | 92 | 24 | 0.9 | 0.7780 | 0.042 | 119 | 1 | 4.4 |
| 18JB55 | N11.3.1 | −71.56 | −62.82 | This study | 112 | 5 | 0.9 | 0.8132 | 0.014 | 112 | 1 | 1.6 |

All the ages were obtained by LA-ICP-MS U–Pb analysis.

$^{207}Pb/^{206}Pb$ initial ratio was constrained by the Tera–Wasserburg concordia upper intercept. Several results have large uncertainties (up to ±26 Ma) owing to the high common to radiogenic Pb ratios in the apatites and a resultant small spread in U/Pb ratio with some analyses clustering close to the *y*-axis of the Tera–Wasserburg concordia. Nevertheless, most apatites have relatively high U concentrations (>20 U ppm) and yield useful uncertainties that are lower than ±7 Ma (Table 1).

A comparison of the zircon U–Pb crystallization age and the apatite lower intercept $^{206}Pb/^{238}U$ age (Fig. 4) reveals an approximately linear 1:1 correlation for rocks with zircon U–Pb crystallization ages younger than *c.* 156 Ma, suggesting that these apatite U–Pb ages record rapid cooling (thermal relaxation) following magmatic crystallization. On the other hand, rocks that crystallized before *c.* 156 Ma yield apatite $^{238}U/^{206}Pb$ lower intercept ages of *c.* 147–128 Ma (Fig. 4). Significantly, four of the five samples that yield apatite Tera–Wasserburg lower intercepts with MSWD > 2 come from rocks that crystallized at *c.* 153 Ma and older. The origin of this elevated dispersion is discussed in the section 'Thermal histories of Mesozoic arc crust through 550–380°C'.

### *Whole-rock geochemistry*

Whole-rock major oxides, trace element and REE concentrations have been determined in the same 36 rocks that were dated using the zircon U–Pb method (Supplementary material Table 1). The majority of the Cretaceous plutonic rocks are classified as alkali granite to granodiorite in the cationic scheme of de La Roche *et al.* (1980; Fig. 5a), although a few diorites, gabbros and olivine gabbros were also sampled. The Early Cretaceous intrusions span the calcic and alkali–calcic differentiation trends on the modified alkali–lime index of Peacock (1931; Fig. 5b). The two Late Cretaceous rocks have calc-alkaline to alkali–calcic compositions (Fig. 5b). The Cretaceous rocks yield aluminium saturation indices (ASI) (Maniar and Piccoli 1989) that straddle the metaluminous–peraluminous fields, and range between 0.74 and 1.61 (Fig. 5c), with no relationship to crystallization age. Normal mid-ocean ridge basalt (N-MORB) normalized trace element abundances (Fig. 5d) reveal no distinct changes through the Cretaceous, with an enrichment in large ion lithophile elements (LILE), and negative Nb, Ta and Ti anomalies, suggesting a subduction-derived component in the magma source regions, and that they may have formed within a

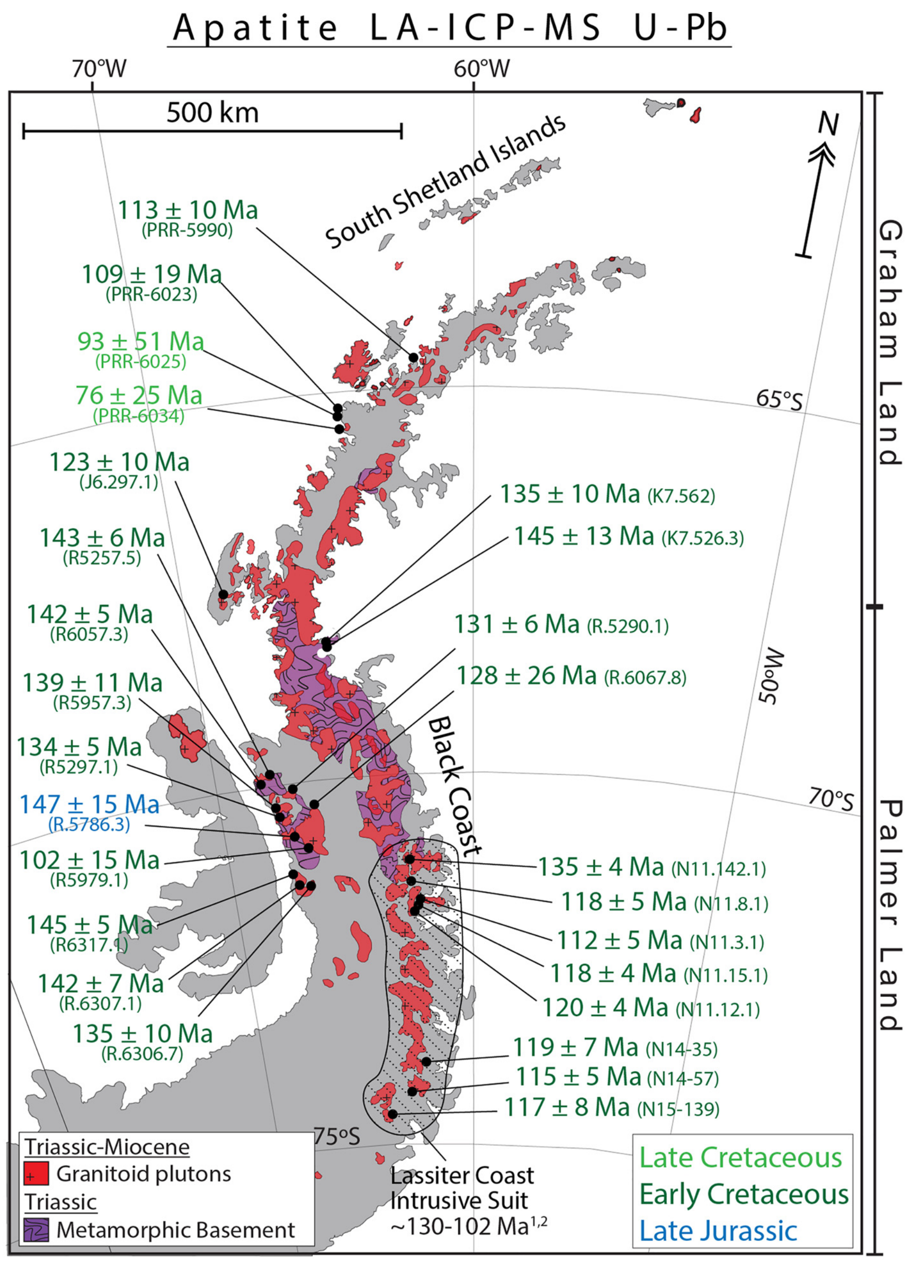


**Fig. 3.** Map of the Antarctic Peninsula, showing the distribution of Jurassic–Neogene intrusive rocks (red) and the Late Triassic Rymill Granite Complex (purple, dotted line), modified from Burton-Johnson and Riley (2015) and Bastias *et al.* (2020). Apatite U–Pb Tera–Wasserburg lower intercept concordia dates acquired from Triassic–Cretaceous igneous rocks are shown. [1]Flowerdew *et al.* (2005); [2]Riley *et al.* (2018).

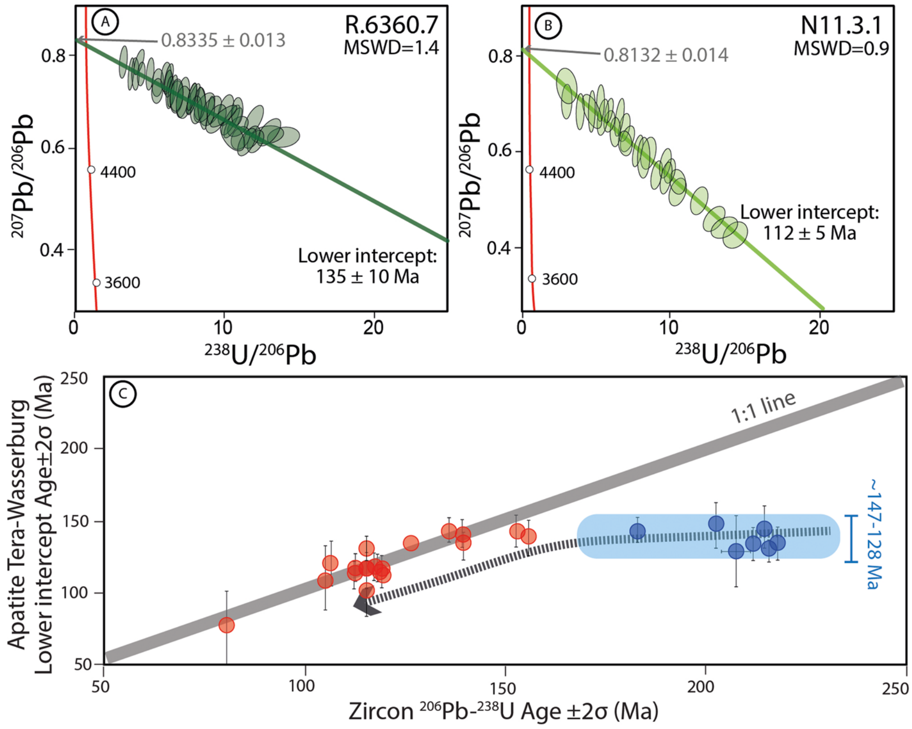


**Fig. 4.** (**a**), (**b**) Representative apatite Tera–Wasserburg concordia plots of the igneous Mesozoic rocks of the Antarctic Peninsula. U–Pb Tera–Wasserburg lower intercept concordia dates are shown. (**c**) Comparison of the zircon U–Pb crystallization ages of Mesozoic igneous rocks of the Antarctic Peninsula and their apatite U–Pb Tera–Wasserburg lower intercept concordia dates. Rocks yielding apatite U–Pb Tera–Wasserburg lower intercept concordia dates that are indistinguishable from their crystallization ages (zircon LA-ICP-MS) are presented in red, otherwise in blue.

continental arc (Fig. 5d). Minor negative Ba, Eu and Sr anomalies, combined with a strong negative Ti anomaly, suggest that plagioclase and Fe–Ti oxides have fractionated, and the positive Pb anomaly is probably derived from an upper crustal source. Trace element concentrations of the Cretaceous rocks normalized to average upper continental crust scatter close to unity (Fig. 5e), supporting a significant crustal origin for the Cretaceous rocks. Tectonic discrimination using (Y + Nb) v. Nb/Y (Whalen and Hildebrand 2019) supports an arc setting for the Cretaceous rocks (Fig. 5f), which is consistent with direct comparisons of Y and Nb (Fig. 5g; Pearce *et al.* 1984). A comparison of Sr/Y v. Y (Fig. 5h) shows that the rocks that formed at *c.* 140–132 and *c.* 92–73 Ma plot in the fields of volcanic arc and adakite, respectively, whereas the rocks that formed during *c.* 126–100 Ma straddle these two fields.

A lack of temporal trends in $La_n/Yb_n$, Sr/Y and Eu/Eu* (Fig. 6) through the Cretaceous suggests that the crustal thickness of the arc did not significantly change during this period (e.g. Hildreth and Moorbath 1988; Mantle and Collins 2008; Chiaradia 2015; Profeta *et al.* 2015). However, we acknowledge that estimates of the thickness of continental arc crust using geochemical indices are problematic owing to the multiple petrogenetic processes that occur in such settings (Ducea *et al.* 2015), and these should perhaps only be used as qualitative indicators (e.g. Kay and Mpodozis 2001; Best *et al.* 2009; Oliveros *et al.* 2019).

### *Sr–Nd-Pb bulk-rock isotopes*

The $^{87}Sr/^{86}Sr_i$ and $\varepsilon Nd_i$ values of the Cretaceous intrusions (139 ± 1 to 79 ± 1 Ma) range between 0.7100 and 0.7040 and +4.1 and −9.7, respectively (Fig. 7). These values reveal no significant trends with time, although $\varepsilon Nd_i$ and $^{87}Sr/^{86}Sr_i$ values span a wider range between *c.* 139 and 112 Ma, compared with the rocks that crystallized between *c.* 112 and 79 Ma (Fig. 7a–c). These data are consistent with the results of Leat *et al.* (2009), who reported from a smaller dataset: (1) $^{87}Sr/^{86}Sr_i$ ratios of 0.70634–0.70563, and $\varepsilon Nd_i$ values of −0.4 and −0.5 from a rock that yields a Rb–Sr isochron date of 132 Ma ± 9 Ma, (2) $^{87}Sr/^{86}Sr_i$ ratios of 0.7080–0.7061 and a $\varepsilon Nd_i$ value of −1.8 from a rock that yields a Rb–Sr isochron date of 116 ± 2 Ma, and (3) $^{87}Sr/^{86}Sr_i$ ratios of 0.7112–0.7044 and $\varepsilon Nd_i$ values ranging between 2.6 and 0.0, from rocks that yield K/Ar dates spanning *c.* 96–71 Ma (Fig. 7a–c). These results yield similar age and Sr isotopic data to previous work (Pankhurst 1982; Pankhurst *et al.* 1991). In addition, Ryan (2007) reported $^{87}Sr/^{86}Sr_i$ ratios between 0.7047 and 0.7045 and $\varepsilon Nd_i$ values ranging between 2.5 and 2.3 from rocks that yield U–Pb zircon dates of 92 ± 1 and 89 ± 1 Ma (Fig. 7a–c).

Whole-rock Pb isotopic compositions of the granitoids that intruded during 139 ± 1 to 79 ± 1 Ma are 19.00–18.31 $(^{206}Pb/^{204}Pb)_i$, 15.67–15.60 $(^{207}Pb/^{204}Pb)_i$ and 38.71–38.05 $(^{208}Pb_i/^{204}Pb_i$; Table 1; Fig. 7d and e), and plot between the upper crust and orogenic curves of Zartman and Doe (1981). There are no significant variations throughout the Cretaceous, although the granitoids that formed during *c.* 126–101 Ma are slightly depleted in $^{208}Pb$ relative to $^{206}Pb$, compared with the older and younger Cretaceous intrusions, and thus they plot slightly closer to upper crustal compositions (Fig. 7e).

### *Zircon* in situ *Hf isotopes*

*In situ* Hf isotopic compositions of zircon have been determined from a suite of the same Cretaceous zircons that were dated using the U–Pb method. Similar to the Nd, Sr and Pb isotopes, there is no systematic variation of $\varepsilon Hf_t$ through the Cretaceous, which varies between +9.3 and −6.4 (Fig. 8). Two Early Cretaceous granitoids (*c.* 139–136 Ma) from the northwestern coast of Palmer Land yield $\varepsilon Hf_t$ values that range from 7.9 to 6.4 and −2.4 to −4.8, respectively. Eleven Aptian–Albian intrusions (126 ± 1 to 101 ± 1 Ma), located in southeastern Palmer Land to northwestern Graham Land and the South Shetland Islands (Fig. 8), yield $\varepsilon Hf_t$ values that range from 9.3 to −6.4. Finally, three Late Cretaceous intrusions (92 ± 1 to 79 ± 1 Ma), yielded $\varepsilon Hf_t$ values that range between 7.9 and −2.2.

The zircons that crystallized during *c.* 139–132 Ma yield a large range of Lu–Hf model ages ($TDM_{Hf}$), which range between 1.07 and 0.36 Ga. Similarly, younger intrusions that formed during 126 ± 1 to 101 ± 1 Ma yield $TDM_{Hf}$ ages that range between 1.14 and 0.27 Ga, whereas the model ages of the Late Cretaceous intrusions lie between 0.89 and 0.32 Ga. The full dataset is presented in Supplementary material Table 4.

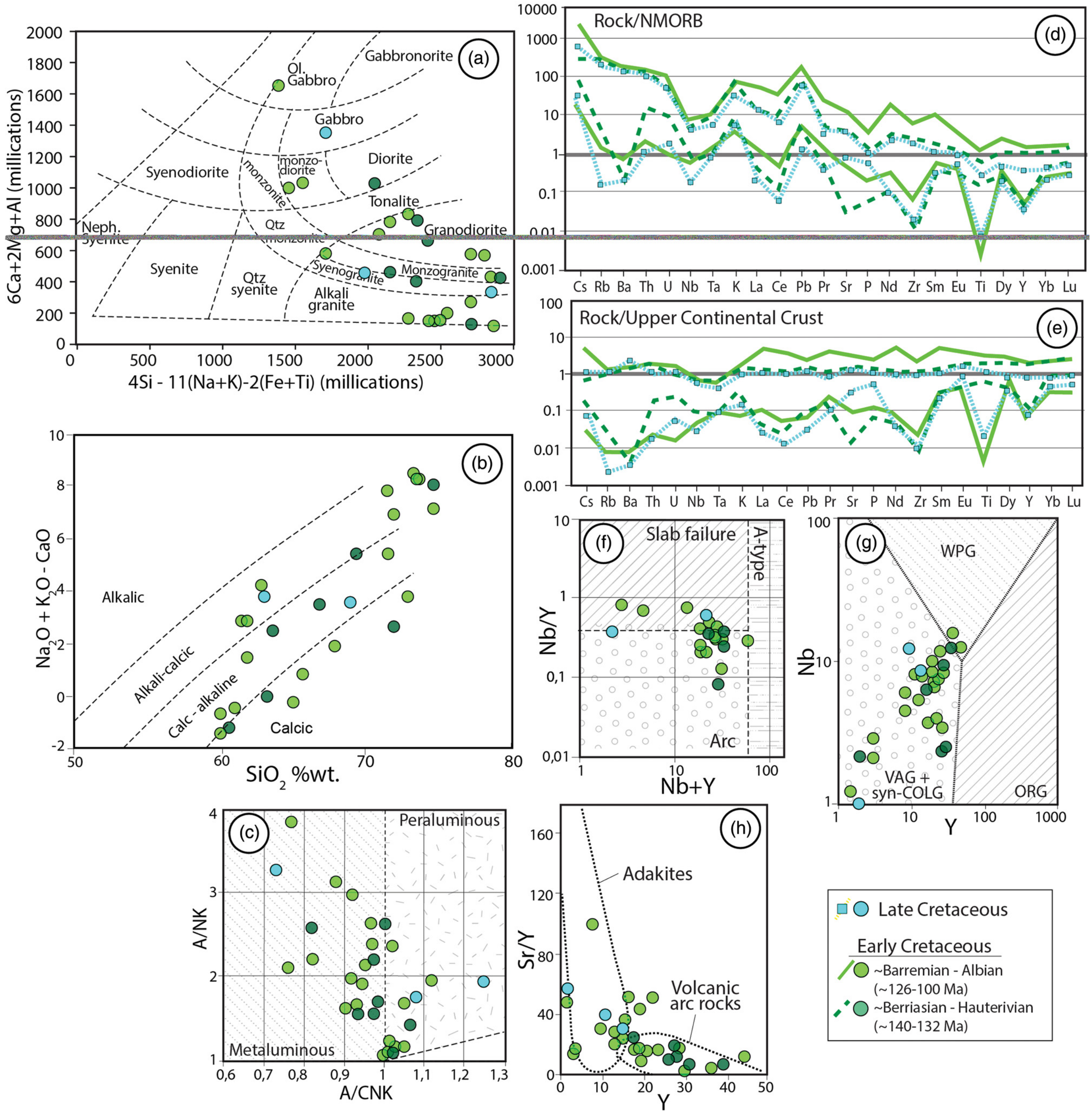


**Fig. 5.** Geochemical compositions of Cretaceous igneous rocks from the Antarctic Peninsula, divided into time slices at *c.* 140–132 Ma (dark green), *c.* 126–100 Ma (light green), and Late Cretaceous (turquoise). (**a**) Multi-cation discrimination plot from de La Roche *et al.* (1980). (**b**) $Na_2O + K_2O - CaO$ v. $SiO_2$ classification diagram of Peacock (1931). (**c**) Molar Al/(Na + K) and Al/(Ca + Na + K) are defined as molecular ratios and take into account the presence of apatite so that rocks with ASI > 1.0 are corundum normative and are termed peraluminous. (**d**) Rare earth element and trace element abundances normalized to N-MORB (Sun and McDonough 1989). (**e**) Trace element abundances normalized to upper continental crust (Taylor and McLennan 1995). (**f**) Nb + Y v. Nb/Y diagram of Hildebrand *et al.* (2018) to differentiate magmatic arc and slab failure (slab break-off) environments. (**g**) Tectonic discrimination diagram of Pearce *et al.* (1984) based on a comparison of Y and Nb. ORG, ocean ridge granites; VAG, volcanic arc granites; WPG, within-plate granites. (**h**) Discrimination of adakitic and normal volcanic arc rocks (andesites, dacites and rhyolites) based on Sr/Y v. Y of Defant and Drummond (1990).

## Interpretation

### *The origin of Cretaceous magmatism in the Antarctic Peninsula*

Early Cretaceous igneous rocks crystallized between 139 ± 1 and 101 ± 1 Ma, and crop out in eastern Palmer Land, the west coast of northern Palmer Land and along the west coast of Graham Land, and within the South Shetland Islands (Fig. 2a). Late Cretaceous intrusions are more spatially restricted and have been identified along the west coast of the central and northern Antarctic Peninsula, and crystallized between 92 ± 1 and 79 ± 1 Ma. Our compilation (Supplementary material Table 3) of 85 well-constrained crystallization ages (79 U–Pb concordant zircon and six $^{40}Ar/^{39}Ar$ whole-rock plateau dates) shows that Cretaceous arc magmatism peaked at *c.* 118–110 Ma, with minor peaks at *c.* 137–136, *c.* 103–102, *c.* 94–93, *c.* 81–80 and *c.* 71–70 Ma (Fig. 2b), which are consistent with the results of Riley *et al.* (2020*a*) and Jordan *et al.* (2020). However, peak magmatism at *c.* 118–110 Ma revises previous suggestions that Cretaceous magmatism peaked at *c.* 142 Ma (Leat *et al.* 1995) or *c.* 141–129 Ma (Vaughan *et al.* 1998).

Our new geochemical data are consistent with a continental arc setting for the Cretaceous igneous rocks of the Antarctic Peninsula.

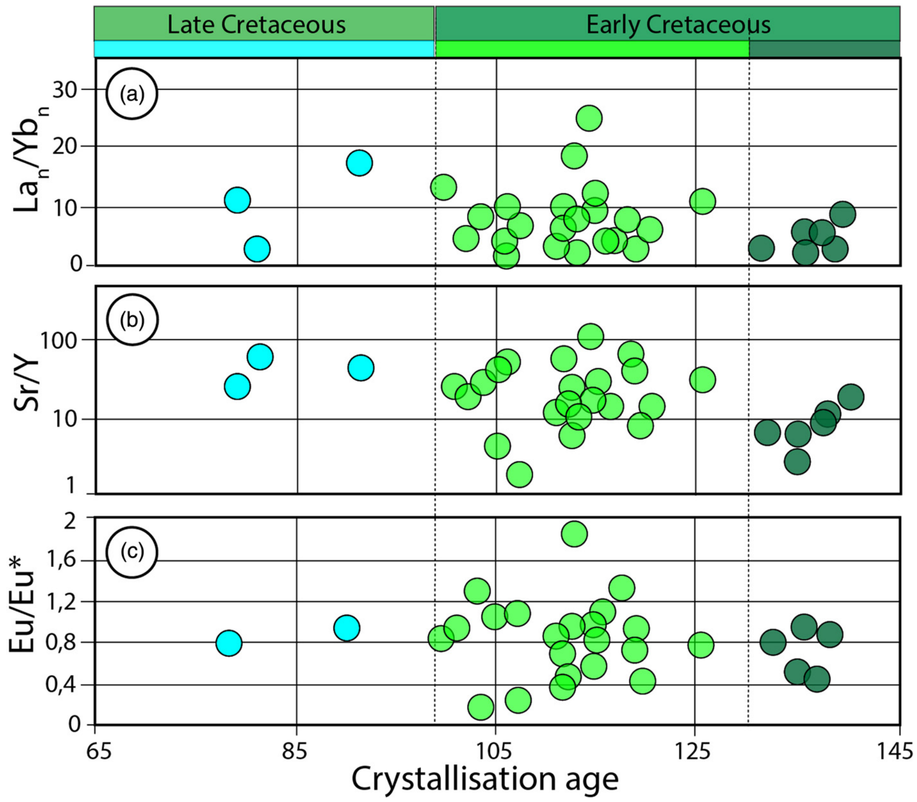


**Fig. 6.** The temporal evolution of some geochemical indexes at *c.* 140–132 Ma (dark green), *c.* 126–100 Ma (light green), Late Cretaceous (yellow). (**a**) $La_n/Yb_n$. (**b**) Sr/Y. (**c**) Eu/Eu* = $Eu_n/(Sm_n*Gd_n)^{1/2}$.

An arc interpretation is supported by (1) the geographical distribution of intrusions that are generally parallel to the margin (Fig. 2a), (2) enriched N-MORB normalized LILE and light REE (LREE), with negative Nb, Ta and Ti anomalies (Fig. 5d), which are typically associated with slab-dehydration reactions at active margins, and (3) whole-rock Nd, Sr and Pb (Fig. 7a, b, d and e), and zircon Hf isotopic compositions (Fig. 8) of Cretaceous igneous rocks that show that the magmas formed from mixed sources within the continental crust, which is common in continental arc settings (e.g. Stern 2002). This is consistent with previous interpretations (e.g. Leat *et al.* 1995; Riley *et al.* 2018, 2020*a*) of the Cretaceous intrusions in the Antarctic Peninsula. Our results also reveal no temporal geochemical or isotopic (Nd, Sr, Pb and Hf) trends through the Cretaceous.

### *Thermal histories of Mesozoic arc crust through 550–380°C*

Igneous rocks that yield zircon U–Pb concordia ages between *c.* 156 ± 1 and *c.* 81 ± 1 Ma yield lower intercept apatite concordia dates ($^{206}Pb/^{238}U$) on Tera–Wasserburg plots that are indistinguishable from their zircon $^{238}U$–$^{206}Pb$ concordia ages (Fig. 4), suggesting that they cooled to below *c.* 380°C rapidly after magmatic intrusion. In contrast, apatites from older intrusions that yield zircon U–Pb concordia dates between *c.* 217 and *c.* 184 Ma yield significantly younger apatite lower intercept concordia dates ($^{206}Pb/^{238}U$), consistently *c.* 147 to *c.* 128 Ma. These apatite dates are interpreted to record cooling through the Pb-in-apatite partial retention zone (*c.* 550–380°C; e.g. Cochrane *et al.* 2014; following the Pb-in-apatite diffusion parameters of Cherniak *et al.* 1991) during *c.* 147–128 Ma. The older plutonic samples (zircon dates between *c.* 217 and *c.* 184 Ma) yield apatite lower intercept ages with slightly elevated MSWD values compared with the apatite intercept ages from the younger igneous rocks (zircon dates between *c.* 156 ± 1 and *c.* 81 ± 1 Ma). This slight dispersion is considered to be a consequence of (i) partial diffusive loss of Pb during cooling through the Pb-in-apatite partial retention zone, and (2) laser sampling of intra-grain regions that were more retentive (e.g. cores of large grains) or less retentive (e.g. small grains or rims of large grains) of Pb.

The older rocks that yield U–Pb zircon ages of *c.* 217 to *c.* 184 Ma and apatite U–Pb ages of *c.* 147–128 Ma form parts of intrusions that are dispersed over a distance of *c.* 400 km (Fig. 3), and thus reveal a regional magmatic emplacement event and subsequent cooling that affected most of the Antarctic Peninsula. Poblete *et al.* (2011) reported significant remagnetization of pre-Jurassic igneous and sedimentary rocks on the Antarctic Peninsula, which would require temperatures of at least 500°C (Hunt *et al.* 1995). This same event was probably responsible for heating the intrusions that formed during *c.* 217 and *c.* 184 Ma to temperatures higher than the apatite Pb partial retention zone, which then subsequently cooled through *c.* 550–380°C at *c.* 147–128 Ma. The cause(s) of the heating event is unclear, although we hypothesize that it may be due to burial and high heat flow. Jurassic turbidite-like deposits exposed along the west coast of the Antarctic Peninsula in Adelaide and Alexander Island (Riley *et al.* 2012) and South Shetland Islands (Bastias *et al.* 2019) may be evidence for the formation of depocentres and burial during this period.

The narrow spread in U–Pb apatite dates (147–128 Ma) from plutons that crystallized during 217–185 Ma suggests that these record a general phase of Early Cretaceous cooling through the apatite Pb partial retention zone (e.g. Cochrane *et al.* 2014), which may be a consequence of tectonic exhumation. However, the driving mechanism for Early Cretaceous tectonic exhumation of the Antarctic Peninsula is unclear and our interpretation is speculative. The Early Cretaceous Andean margin experienced rock uplift and erosion during the Early Cretaceous during westward migration of South America, induced by the opening of the South Atlantic (e.g. Mpodozis and Ramos 1989). Additionally, ridge formation is also recorded in the Weddell Sea (e.g. König and Jokat 2006) and Rocas Verdes (e.g. Calderón *et al.* 2007), located in the South Atlantic and Patagonia, respectively. Tectonic exhumation related to the opening of the Atlantic Ocean has been already suggested for the western

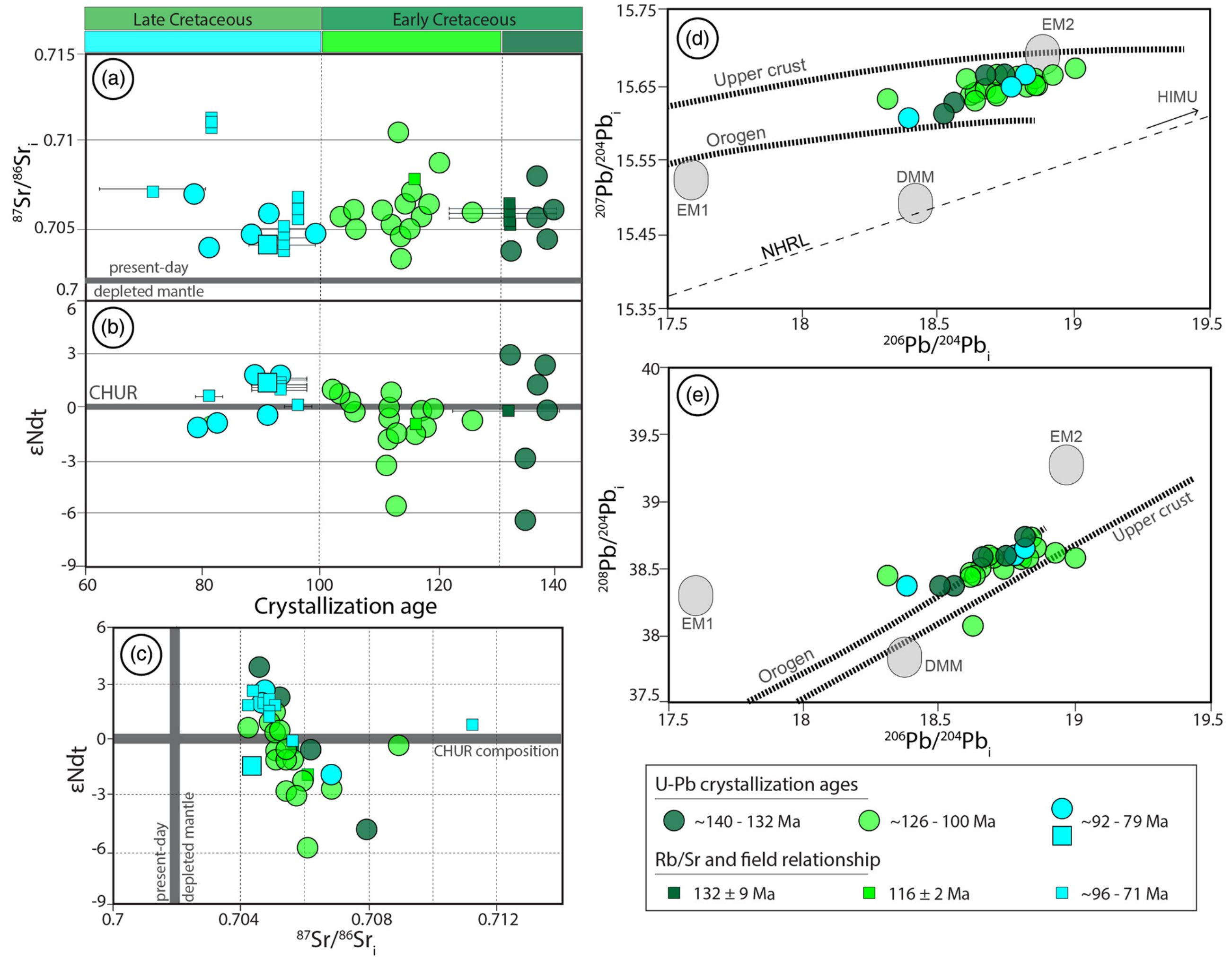


**Fig. 7.** Whole-rock isotopic compositions of Cretaceous igneous rocks of the Antarctic Peninsula at *c.* 140–132 Ma (dark green), *c.* 126–100 Ma (light green) and Late Cretaceous (turquoise). (**a**, **b**) Temporal evolution of whole-rock (**a**) $^{87}Sr/^{86}Sr_i$ and (**b**) $\varepsilon Nd_t$. Data are reported only from samples that are considered to yield accurate crystallization ages. (**c**) Comparison of the $\varepsilon Nd_t$ and $^{87}Sr/^{86}Sr_i$ values that are shown in (**a**) and (**b**). The full dataset is a combination of data from this study and data (Rb–Sr, $^{40}Ar/^{39}Ar$, U–Pb zircon and field relationships) from Late Cretaceous rocks presented by Ryan (2007) and Leat *et al.* (2009). (**d**, **e**) Pb isotopic compositions of the Cretaceous igneous whole-rocks showing the lead-isotope evolution curves of Zartman and Doe (1981) for upper crust and orogen. Approximate composition of EM1 (enriched mantle with recycled lower continental crust), EM2 (enriched mantle with upper continental crust and continental derived sediments) and DMM (depleted MORB-mantle) are from Hanan and Graham (1996) and Stracke *et al.* (2003). HIMU, high U/Pb mantle composition. NHRL, Northern Hemisphere Reference Line (Dupre and Allègre 1980).

margin of Patagonia during the Mesozoic (Homovc and Constantini 2001). Furthermore, Gianni *et al.* (2018, 2020) reported Early Cretaceous compression in Patagonia, and Sarmiento and Rangel (2004), Martin-Gombojav and Winkler (2008), Villagómez and Spikings (2013) and Spikings *et al.* (2015) reported compression and exhumation of the Colombian and Ecuadorian margin during *c.* 120–110 Ma, leading to the emplacement of HP–LT complexes (e.g. Raspas Complex; Spikings *et al.* 2015). It is noteworthy that HP–LT rocks are also exposed along the South Shetland Islands (Smith Island; e.g. Grunow *et al.* 1992) within the Antarctic Peninsula, and they reside in the same structural position to the west of the Mesozoic intrusions as they do elsewhere in the Andes. Therefore, it is feasible to suggest, pending future work, that these HP–LT rocks were exhumed during Early Cretaceous compression.

Summarizing, we suggest that the small variation in apatite U–Pb dates in plutons that crystallized during *c.* 217 to *c.* 184 Ma reflects Late Jurassic–Early Cretaceous burial, followed by tectonic exhumation caused by the early opening of the Atlantic Ocean. This event is not recorded by the younger plutons (*c.* 156–81 ± 1 Ma) because these were probably cooler than the apatite Pb partial retention zone prior to the exhumation event.

### *Sources of magmatism, magma addition rates and petrogenesis*

The general uniformity in whole-rock geochemical compositions (Figs 5 and 6) suggests that there were no significant changes in tectonic setting during *c.* 140 and *c.* 79 Ma. The exhumation phase identified by the apatite U–Pb data may have been slow, and did not result in significant changes in crustal thickness. The intrusions are mostly calcic and alkali–calcic alkali-granite and granodiorites that formed in a continental subduction-zone setting (Fig. 5). Exceptions to the general geochemical uniformity of the igneous rocks throughout the Cretaceous consist of the identification of adakite-like magmas in the interval *c.* 126–100 Ma, which immediately followed a period of elevated compression and higher exhumation rates (Fig. 5f), and higher magma addition rates from *c.* 118 to 100 Ma (Fig. 2b).

A comparison of the Hf-isotopic compositions reveals significant differences in the source regions of Cretaceous (this study; Zheng *et al.* 2018; Riley *et al.* 2020*a*) and pre-Cretaceous zircons (Bastias *et al.* 2020, 2021*a*). Zircons from Ordovician to Triassic plutons show a steady trend towards less radiogenic $\varepsilon Hf_t$ values with time (Fig. 9a; Bastias *et al.* 2020). With the exception of a Late Jurassic

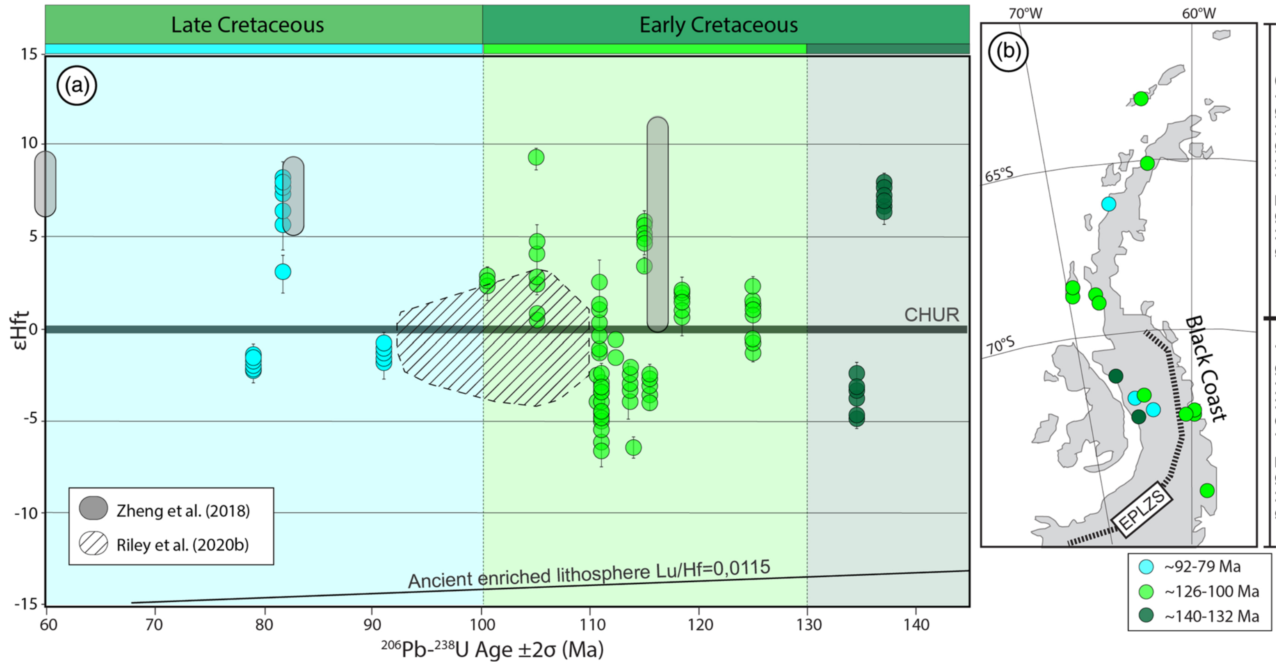


**Fig. 8.** (**a**) Comparison of the $^{206}Pb$–$^{238}U$ zircon concordia ages and zircon $\varepsilon Hf_t$ for grains that crystallized during *c.* 140–132 Ma (dark green), *c.* 126–100 Ma (light green) and approximately Late Cretaceous (turquoise). The 2σ uncertainties are *c.* ±5% for U–Pb zircon ages. (**b**) Present-day map of the Antarctic Peninsula showing the location of the analysed rocks presented in (**a**). Data from Zheng *et al.* (2018) and Riley *et al.* (2020*b*) are included.

granite (sample R.5957.3; Bastias *et al.* 2021*a*, *b*) that yielded $\varepsilon Hf_t$ values between 7.8 and 5.6, Triassic and Jurassic zircons yield broadly similar $\varepsilon Hf_t$ values that range between 0.6 and −9.2 (Fig. 9a; Bastias *et al.* 2020, 2021*a*, *b*). These trends contrast with the Cretaceous zircons, which yield more radiogenic $\varepsilon Hf_t$ values that range between 12.5 and −6.5, revealing the involvement of more radiogenic source regions in the Early Cretaceous. With the exception of granite R.5957.3, Ordovician to Jurassic intrusions yield a consistent range of Lu–Hf model ages that span 1.37 Ga (at *c.* 212 Ma; Bastias *et al.* 2020) to 0.78 Ga (at *c.* 440 Ma; Bastias *et al.* 2020), with the majority ranging between 1.2 and 0.8 Ga (Fig. 9c). This suggests that the Ordovician–Jurassic arc magmas mainly incorporated juvenile Sunsas-aged crust (1.19–0.92 Ga; Cordani and Sato 2000) that is exposed in South America and crust of similar age that is exposed in East Antarctica (1.1–1.0 Ga; Goodge and Fanning 2016). Cretaceous zircons yield Lu–Hf model ages that range between 1.14 Ga (at *c.* 112 Ma) and 0.28 Ga (at *c.* 106 Ma), whereas the majority of Cretaceous zircons yield Lu–Hf model ages of <0.8 Ga (Fig. 9b), suggesting that the structure of the crust may have been modified after the Jurassic, reducing the volume proportion of material derived from Precambrian basement (Fig. 9d).

## *Cretaceous tectonic history*

### *Evidence for a prevailing extensional setting*

The combination of U–Pb zircon dates, geochemical and isotopic data, and mid-temperature thermochronological constraints is consistent with an extensional regime during the Late Jurassic–Early Cretaceous, which may have been interrupted by a mild compressional phase that exhumed the pre-*c.* 184 Ma intrusions during *c.* 147–128 Ma. Evidence for compressive pulses at *c.* 107 and *c.* 103 Ma (Vaughan and Pankhurst 2008; Vaughan *et al.* 2012; Riley *et al.* 2020*a*) has been accounted for by an increase in plate convergence rates. First, Hf-isotopic compositions of zircons show that more isotopically juvenile crust was incorporated into Cretaceous magmas compared with older intrusions, which is in agreement with the interpretation of Pankhurst (1982) based on Sr isotopes. Extension may have driven decompression of the underlying mantle, promoting the incorporation of mantle melts into the arc magmas (e.g. Cochrane *et al.* 2014). Second, re-magnetization of pre-Jurassic igneous and sedimentary rocks (Poblete *et al.* 2011), along with resetting of apatite U–Pb dates (via diffusive Pb loss) was probably caused by increased heat flow and burial during extension (e.g. Lachenbruch *et al.* 1994). Finally, synchronous extension has been recorded in adjacent regions of the Antarctic Peninsula throughout most of the Cretaceous, which was related to the break-up of Gondwana. Oceanic lithosphere formed in the Weddell Sea at c. 147 Ma, outboard of the northeastern Antarctic Peninsula (Fig. 1a; König and Jokat 2006), which led to the opening of the Southern Atlantic. An extensional setting is also documented along the western margin of Patagonia, where it formed the Rocas Verdes Basin, a marginal back-arc basin that developed oceanic lithosphere during the Late Jurassic to Cretaceous (e.g. Dalziel *et al.* 1974; Dalziel 1981; Calderón *et al.* 2007). Moreover, most of the South American western margin was dominated by an extensional setting during the Late Jurassic–Early Cretaceous (e.g. Atherton and Aguirre 1992; Mpodozis and Allmendinger 1993; Morata and Aguirre 2003; Spikings *et al.* 2015).

### c. *148–140 Ma: magmatic quiescence*

The period between *c.* 148 and 140 Ma is characterized by magmatic quiescence along the entire length of the Antarctic Peninsula. Most Late Paleozoic–Jurassic plate reconstructions show subduction of Pacific oceanic lithosphere beneath the western margin of Gondwana at this time (e.g. Meert and Lieberman 2008; Nelson and Cottle 2017, 2018) and thus the mechanism responsible for this quiescence remains unclear, although it may indicate high convergence obliquity or a lack of net convergence.

### c. *140–100 Ma: oceanic subduction*

Arc magmatism resumed along the Antarctic Peninsula in the Berriasian–Valanginian transition (*c.* 140 Ma; Fig. 10) owing to

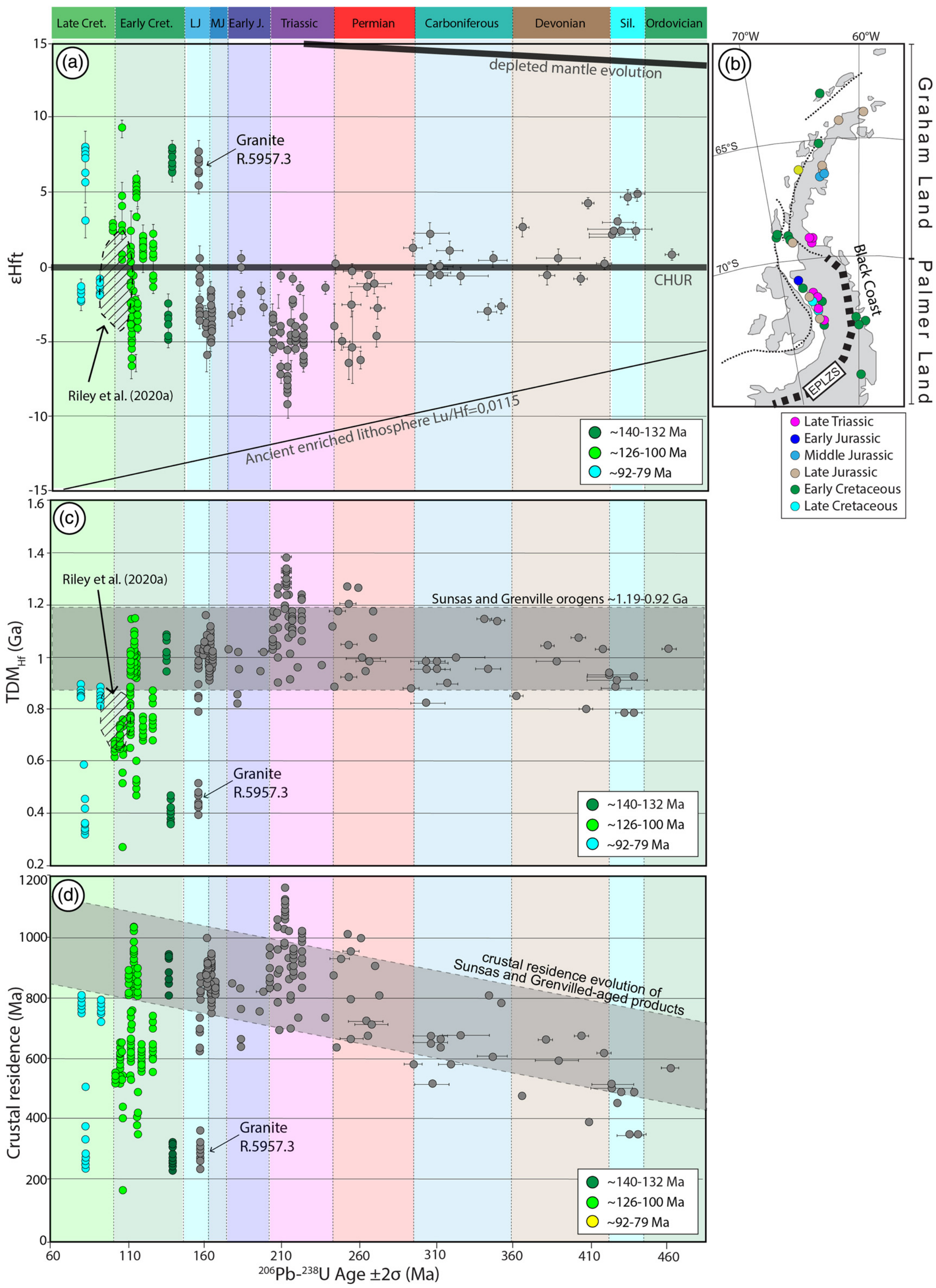


**Fig. 9.** (**a**) Comparison of $^{206}Pb$–$^{238}U$ zircon concordia ages and zircon $\varepsilon Hf_t$ for grains extracted from Mesozoic igneous rocks of the Antarctic Peninsula (this study; Bastias *et al.* 2020, 2021*a*, *b*). The 2σ uncertainties are *c.* ±5% for U–Pb zircon ages. (**b**) Present-day map of the Antarctic Peninsula showing the location of the analysed rocks presented in (**a**). (**c**) Comparison of the $^{206}Pb$–$^{238}U$ zircon concordia ages and the Lu–Hf model ages (this study; Bastias *et al.* 2020, 2021*a*). (**d**) Comparison of $^{206}Pb$–$^{238}U$ zircon concordia ages and crustal residence, which is defined as the difference between the zircon U–Pb crystallization age and the $TDM_{Hf}$ age. The Cretaceous dataset is divided into *c.* 140–132 Ma (dark green), *c.* 126–100 Ma (light green) and approximately Late Cretaceous (turquoise). Data from Riley *et al.* (2020*a*) are included.

subduction of the Phoenix Plate. Magmatic pulses occurred at *c.* 137–136, *c.* 118–110 and *c.* 103–102 Ma (Fig. 2b), although the margin was continuously active throughout the Early Cretaceous, corroborating previous studies (e.g. Leat *et al.* 1995; Riley *et al.* 2018). Early Cretaceous intrusions include the Lassiter Coast Intrusive Suite in eastern Palmer Land, and the west coast of southern Graham Land in the Black Coast sector. Further north, arc magmatism from *c.* 140 to 100 Ma occurs along the west coast of Graham Land up to its northernmost exposure in the South Shetland Islands (Fig. 2a). This geographical distribution of Early Cretaceous

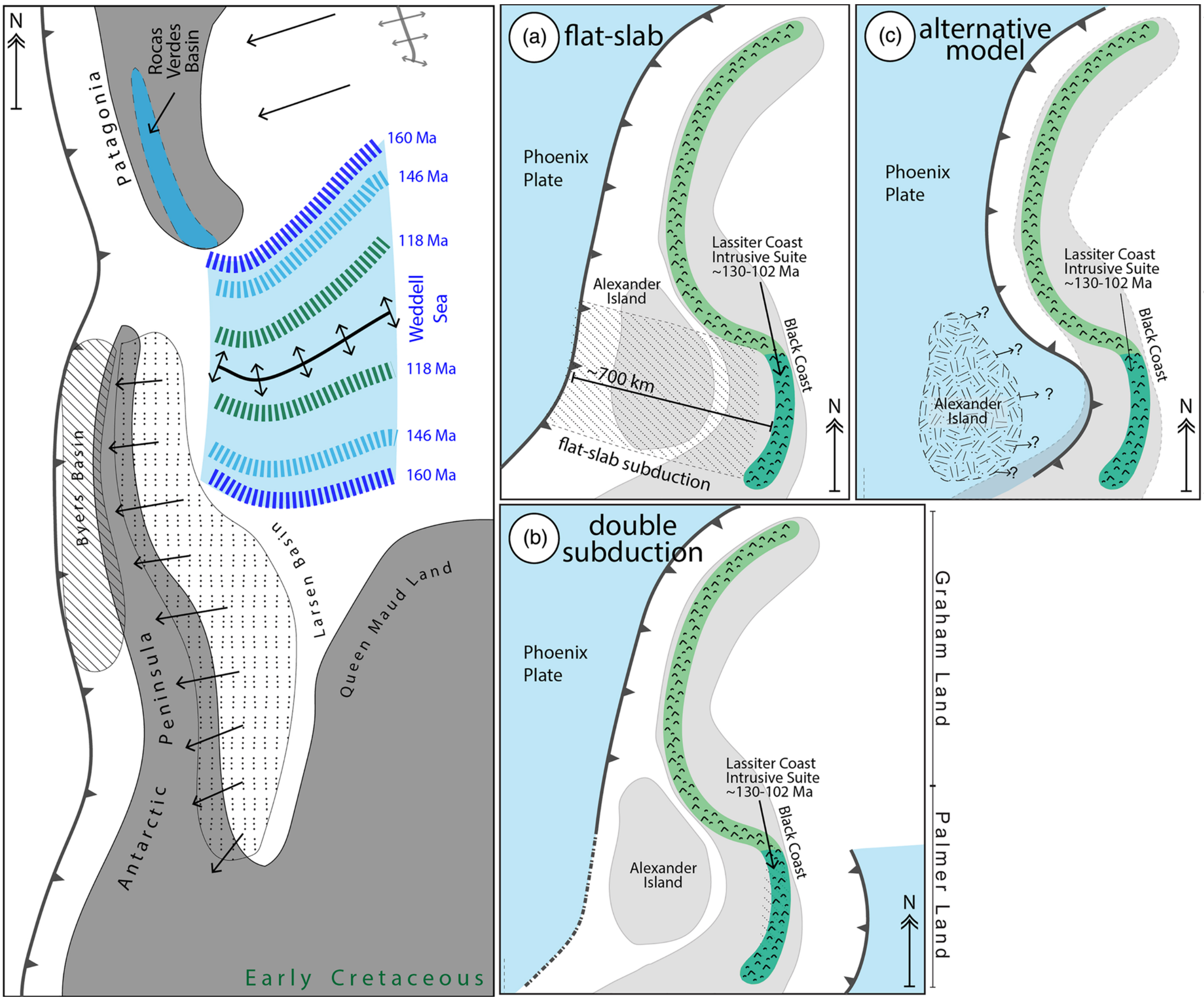


**Fig. 10.** Schematic palaeo-reconstruction of western Gondwana including the Antarctic Peninsula and Patagonia during the Early Cretaceous, showing the Rocas Verdes Basin (*c.* 152–142 Ma; Calderón *et al.* 2007), Byers Basin (Bastias *et al.* 2019), Larsen Basin (Hathway 2000), and the Weddell Sea including the magnetic anomalies of Ghidella *et al.* (2002). Arrows in the Antarctic Peninsula indicate drift direction owing to the opening of the Weddell Sea. Different geodynamic scenarios are proposed: (**a**) continuous east-dipping subduction of the Phoenix Plate beneath the Antarctic Peninsula with a low-angle subducted sector at the latitude of Alexander Island; (**b**) double subduction beneath the Antarctic Peninsula; (**c**) continuous subduction of the Phoenix Plate beneath the western Antarctic Peninsula and an allochthonous or parautochthonous origin of the crustal block of Alexander Island.

igneous rocks from *c.* 140 to 100 Ma could be accounted for by either flat-slab, east-dipping subduction of the Phoenix Plate, west-dipping subduction of the lithosphere of the Weddell Sea, or an allochthonous origin for the rocks of Alexander Island, each of which is discussed below.

*Flat slab*. Most Early Cretaceous palaeogeographical reconstructions show east-dipping subduction of oceanic lithosphere of the Phoenix Plate beneath the Antarctic Peninsula (e.g. Barker 1982; Larter and Barker 1991; Sutherland and Hollis 2001; Jordan *et al.* 2020). Assuming that the rocks of Alexander Island are autochthonous to the Antarctic Peninsula and there was no significant strike-slip displacement along the margin, this implies a distance of *c.* 700 km between the trench and arc rocks of the Lassiter Coast Intrusive Suite (Fig. 10a), which have a trench-parallel extent of at least *c.* 300 km. Consequently, in this scenario the rocks of the Lassiter Coast Intrusive Suite (*c.* 130–102 Ma; Pankhurst *et al.* 1991; Riley *et al.* 2018) formed above a flattened slab (Fig. 10a). To the north of the Black Coast, igneous rocks were emplaced along the west coast of the Antarctic Peninsula, suggesting that the extent of the flat slab was constrained to a segment of Palmer Land (Fig. 10a).

*West-dipping subduction*. Arc rocks of the Lassiter Coast Intrusive Suite of eastern Palmer Land may have formed within an active margin associated with west-dipping subduction of lithosphere of the Weddell Sea beneath eastern Palmer Land (Fig. 10b). This hypothesis was proposed by Grunow (1993), who suggested that counterclockwise rotation of the Antarctic Peninsula during the Jurassic in conjunction with the general southward motion of East Antarctica may have driven west-dipping subduction. However, this hypothesis is inconsistent with palaeogeographical reconstructions based on seafloor magnetic anomalies in the Weddell Sea region (e.g. Ghidella *et al.* 2002, 2007; Jokat *et al.* 2003; König and Jokat 2006), and the accommodation of lithosphere that may have been subducted during *c.* 140–100 Ma. Extension in the South Atlantic leading to the development of seafloor spreading and the formation of the Weddell Sea occurred during the Late Jurassic (e.g. Ghidella *et al.* 2002); most of this seafloor is still present to the east of the Scotia Plate (Fig. 2a; Ghidella *et al.* 2002, 2007; König and Jokat 2006), and thus poses a problem when trying to account for subduction east of Palmer Land. However, this argument is not conclusive, considering that the age of significant portions (e.g. the southern sector) of the Weddell Sea remains unknown; therefore west-dipping subduction remains a possibility.

*An allochthonous origin for Alexander Island*. The present sinuous spatial trend of Early Cretaceous magmatism (*c.* 140–100 Ma) may be a consequence of post *c.* 100 Ma bending and rotation of the peninsula, implying that the original Early Cretaceous arc was parallel to the ocean–continent interface, with an approximately similar, trench-parallel arc–trench gap. This hypothesis also requires that Alexander Island is part of an allochthonous or parautochthonous crustal block that was located elsewhere prior to *c.* 100 Ma, and that the Early Cretaceous trench would have been located close to the present position of George VI Sound (Fig. 10c). In this model, Alexander Island arrived close to its present position after *c.* 100 Ma. However, Alexander Island hosts Mesozoic forearc sequences (Fossil Bluff Group; Butterworth *et al.* 1988), which have been chronologically and lithostratigraphically correlated with Mesozoic forearc sequences further north in Adelaide Island (Riley *et al.* 2012) and in the South Shetland Islands (Bastias *et al.* 2019). Thus, an allochthonous origin for Alexander Island suggests that it may have been accreted along the west Antarctic margin via displacement along the Eastern Palmer Land Shear Zone (Fig. 2a), which is a major ductile to brittle–ductile shear zone with a lateral extent of at least 1500 km (Vaughan and Storey 2000; Vaughan *et al.* 2012; Fig. 2). Translation of Alexander Island and emplacement close to its current location would have occurred after *c.* 100 Ma, although U–Pb zircon and $^{40}Ar/^{39}Ar$ biotite dates of syntectonic intrusions within this shear zone suggest that it was active during *c.* 106–102 Ma (Vaughan *et al.* 2002*a*, *b*), and there is no evidence for displacement since *c.* 102 Ma.

### c. *100–79 Ma*

Exposures of Late Cretaceous igneous rocks are less voluminous than the Early Cretaceous units (Fig. 2a) and occur along the west coast of the central and northern Antarctic Peninsula (Fig. 11). Late Cretaceous igneous rocks in Graham Land formed with similar trench–arc distances at its west coast. However, arc magmas migrated westward during the Late Cretaceous–Paleogene at the latitude of northern Alexander Island in Palmer Land (Pankhurst 1982; Storey *et al.* 1996; McCarron and Millar 1997; Riley *et al.* 2020*a*). The absence of Late Cretaceous or Paleogene intrusive rocks at the latitudes of the Lassiter Coast Intrusive Suite suggests that subduction had ceased at *c.* 112 Ma in more southerly latitudes, which probably signals subduction of the last remaining oceanic lithosphere of the Phoenix Plate under the margin of the Antarctic Peninsula (e.g. Barker 1982; Larter and Barker 1991).

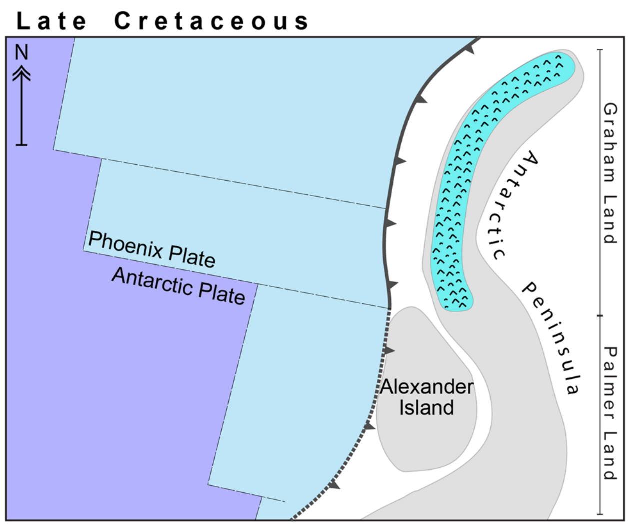


**Fig. 11.** Schematic palaeo-reconstruction of the Antarctic Peninsula during the Late Cretaceous. The margin was dominated by west-dipping subduction of oceanic lithosphere of the Phoenix Plate. A lack of Late Cretaceous arc magmatism in the southern Antarctic Peninsula suggests that the margin was inactive. Active margin magmatism continued along Graham Land during the Late Cretaceous.

## Conclusions

(1) Arc magmatism resumed in the Antarctic Peninsula at *c.* 140 Ma following a magmatic hiatus during the interval *c.* 148–140 Ma, forming abundant intrusions that are exposed along Graham and Palmer Land. Magmatism was continuous until *c.* 79 Ma, with the main peak of activity at *c.* 118–110 Ma, which represents one of the main periods of Mesozoic magmatism in the Antarctic Peninsula. This magmatism was formed within a continental active margin setting, which is supported by (a) the trench-parallel distribution of the igneous rocks, (b) chemical compositions that reveal an enrichment in LILE and LREE, with negative Nb, Ta and Ti anomalies, which are typical of slab-dehydration reactions and thus active margins, and (c) whole-rock Nd and Sr and zircon Hf isotopic compositions revealing mixed sources that resided within the continental crust.

(2) Apatite U–Pb dates show that intrusions that crystallized during *c.* 217 and *c.* 184 Ma within the Antarctic Peninsula cooled through the Pb-in-apatite partial retention zone (*c.* 550–380°C) during *c.* 147–128 Ma. First, these intrusions were probably heated to temperatures hotter than *c.* 550°C via increased flow and burial during Late Jurassic–Early Cretaceous extension, which also remagnetized the pre-Jurassic igneous and sedimentary rocks of the Antarctic Peninsula. Subsequent cooling may have been a consequence of exhumation driven by compression and rock uplift, caused by the westward migration of South America during the early opening of the South Atlantic.

(3) An overall extensional setting during the Cretaceous is supported by (a) progressively more radiogenic $\varepsilon$Hf compositions of Cretaceous zircons revealing the incorporation of mantle melts during attenuation of the crust and (b) evidence for high Late Jurassic to Cretaceous heat flow that magnetized pre-Jurassic rocks and reset apatite U–Pb ages of pre-Middle Jurassic rocks. However, this extensional period was punctuated by compressive events, the most pronounced of which may have been at the beginning of the Early Cretaceous (see conclusion (2)).

(4) Early Cretaceous exposures of arc rocks crop out from the east to the west coast at the latitude of the Black Coast in Palmer Land. This spatial trend may be due to either (a) continuous subduction beneath the western margin of the Antarctic Peninsula with a flat-slab episode in Palmer Land, or (b) east-dipping subduction of the Phoenix Plate in Graham Land and west-dipping subduction in Palmer Land, or (c) an active western margin with east-dipping subduction of the Phoenix Plate, along with an allochthonous or parautochthonous origin for Alexander Island. Our current dataset is unable to distinguish between these possibilities, and testing these hypotheses would require a better understanding of the geological history of the pre-Cretaceous rocks of Alexander Island and the inaccessible areas of the Weddell Sea in the Filchner–Ronne Ice Shelf sector.

(5) The geochemical and isotopic compositions of the Late Cretaceous arc rocks are extremely similar to their Early Cretaceous counterparts. Therefore, we suggest that active margin magmatism was continuous throughout the Cretaceous in the Antarctic Peninsula, which is consistent with previous studies (e.g. Leat *et al.* 1995; Riley *et al.* 2020*a*). Late Cretaceous arc magmatism occurred during the closing stages of subduction of the oceanic lithosphere of the Phoenix Plate in Palmer Land, which gradually

ceased moving northward throughout the Cenozoic (e.g. Barker 1982; Larter and Barker 1991).

**Acknowledgements** We are grateful for the logistical support provided by the Instituto Antártico Chileno (INACH) during two field campaigns to the Antarctic Peninsula. We thank the British Antarctic Survey and the Polar Rock Repository of the Byrd Polar and Climate Research Center, who provided access to their sample archive. Technical support was provided by the staff and laboratories of the Isotope Geochemistry Group of the University of Geneva. M. Ghiglione is thanked for editorial handling, and the authors are grateful to D. Rojo, R. Pankhurst and an anonymous reviewer for providing constructive criticism that improved the paper.

**Author contributions** **JB**: conceptualization (lead), data curation (lead), formal analysis (lead), funding acquisition (lead), investigation (lead), methodology (lead), project administration (lead), resources (lead), software (lead), validation (lead), visualization (lead), writing – original draft (lead), writing – review & editing (lead); **RS**: data curation (equal), formal analysis (equal), funding acquisition (lead), investigation (lead), methodology (equal), project administration (equal), supervision (lead), writing – original draft (lead), writing – review & editing (lead); **TR**: data curation (equal), investigation (equal), writing – review & editing (equal); **DC**: data curation (equal), formal analysis (equal), funding acquisition (lead), investigation (lead), software (lead), supervision (equal), validation (lead), writing – original draft (equal), writing – review & editing (equal); **AG**: data curation (lead), supervision (equal); **AU**: data curation (lead), investigation (supporting), methodology (equal); **MC**: data curation (equal), investigation (equal), validation (equal); **AB-J**: data curation (supporting)

**Funding** This research was funded by the Instituto Antártico Chileno (INACH, project RT-06-14) and the University of Geneva. J.B. acknowledges support from a PhD scholarship of ANID-Chile and the Swiss National Science Foundation (project P500PN_202847). D.C. acknowledges support from Science Foundation Ireland under Grants 13/RC/2092 and 13/RC/2092_P2.

**Competing interests** The authors declare that they have no known competing financial interests or personal relationships that could have appeared to influence the work reported in this paper.

**Data availability** All data generated or analysed during this study are included in this published article (and its supplementary information files). Further details can be shared by personal communication with the authors.

*Scientific editing by Matias Ghiglione*

## References


Atherton, M.P. and Aguirre, L. 1992. Thermal and geotectonic setting of Cretaceous volcanic rocks near Ica, Peru, in relation to Andean crustal thinning. *Journal of South American Earth Sciences*, **5**, 47–69, https://doi.org/10.1016/0895-9811(92)90059-8

Barker, P. 1982. The Cenozoic subduction history of the Pacific margin of the Antarctic Peninsula: ridge crest–trench interactions. *Journal of the Geological Society, London*, **139**, 787–801, https://doi.org/10.1144/gsjgs.139.6.0787

Bastias, J. 2014. *Mineralogía y geocronología U–Pb en las Islas Shetland del Sur, Antártica, un multienfoque para Punta Hannah, Isla Livingston y Cabo Wallace, Isla Low*. MS thesis, Universidad de Chile, Santiago, http://www.repositorio.uchile.cl/handle/2250/115611

Bastias, J. 2020. *The Triassic–Cretaceous Tectonomagmatic History of the Antarctic Peninsula Constrained by Geochronology, Thermochronology and Isotope Geochemistry*. Thèse, Université De Genève, https://doi.org/10.13097/archive-ouverte/unige:143280; https://archive-ouverte.unige.ch/unige

Bastias, J., Calderón, M. *et al.* 2019. The Byers Basin: Jurassic–Cretaceous tectonic and depositional evolution of the forearc deposits of the South Shetland Islands and its implications for the northern Antarctic Peninsula. *International Geology Review*, **62**, 1467–1484, https://doi.org/10.1080/00206814.2019.1655669

Bastias, J., Spikings, R. *et al.* 2020. The Gondwanan margin in West Antarctica: insights from Late Triassic magmatism of the Antarctic Peninsula. *Gondwana Research*, **81**, 1–20, https://doi.org/10.1016/j.gr.2019.10.018

Bastias, J., Spikings, R., Riley, T., Ulianov, A., Grunow, A., Chiaradia, M. and Hervé, F. 2021*a*. A revised interpretation of the Chon Aike magmatic province: active margin origin and implications for the opening of the Weddell Sea. *Lithos*, **386–387**, 106013, https://doi.org/10.1016/j.lithos.2021.106013

Bastias, J., Spikings, R., Riley, T., Ulianov, A., Grunow, A., Chiaradia, M. and Hervé, F. 2021*b*. Data on the arc magmatism developed in the Antarctic Peninsula and Patagonia during the Late Triassic–Jurassic: a compilation of new and previous geochronology, geochemistry and isotopic tracing results. *Data in Brief*, **36**, 107042, https://doi.org/10.1016/j.dib.2021.107042

Best, M.G., Barr, D.L., Christiansen, E.H., Gromme, S., Deino, A.L. and Tingey, D.G. 2009. The Great Basin Altiplano during the middle Cenozoic ignimbrite flareup: insights from volcanic rocks. *International Geology Review*, **51**, 589–633, https://doi.org/10.1080/00206810902867690

Boyce, D., Charrier, R. and Farias, M. 2020. The first Andean compressive tectonic phase. Sedimentologic and structural analysis of mid-Cretaceous deposits in the Coastal Cordillera, Central Chile (32°50’S). *Tectonics*, **39**, e2019TC005825, https://doi.org/10.1029/2019TC005825

Bryan, S.E. and Ferrari, L. 2013. Large Igneous Provinces and Silicic Large Igneous Provinces: progress in our understanding over the last 25 years. *Geological Society of America Bulletin*, **125**, 1053–1078, https://doi.org/10.1130/B30820.1

Burton-Johnson, A. and Riley, T.R. 2015. Autochthonous v. accreted terrane development of continental margins: a revised *in situ* tectonic history of the Antarctic Peninsula. *Journal of the Geological Society, London*, **172**, 822–835, https://doi.org/10.1144/jgs2014-110

Burton-Johnson, A., Riley, T., Harrison, R., Mac Niocaill, M., Muraszko, J. and Rowley, P. in press. Tectonic control on episodic magmatic flare-up events revealed by AMS and U–Pb geochronology on the Antarctic Peninsula. *Gondwana Research*.

Butterworth, P.J., Crame, J.A., Howlett, P.J. and Macdonald, D.I.M. 1988. Lithostratigraphy of Upper Jurassic–Lower Cretaceous strata of eastern Alexander Island, Antarctica. *Cretaceous Research*, **9**, 249–264, https://doi.org/10.1016/0195-6671(88)90020-1

Calderón, M., Fildani, A., Hervé, F., Fanning, C.M., Weislogel, A. and Cordani, U. 2007. Late Jurassic bimodal magmatism in the northern sea-floor remnant of the Rocas Verdes Basin, southern Patagonian Andes. *Journal of the Geological Society, London*, **164**, 1011–1022, https://doi.org/10.1144/0016-76492006-102

Castillo, P., Fanning, C.M., Hervé, F. and Lacassie, J.P. 2016. Characterisation and tracing of Permian magmatism in the south-western segment of the Gondwanan margin; U–Pb age, Lu–Hf and O isotopic compositions of detrital zircons from metasedimentary complexes of northern Antarctic Peninsula and western Patagonia. *Gondwana Research*, **36**, 1–13, https://doi.org/10.1016/j.gr.2015.07.014

Cawood, P.A. 2005. Terra Australis Orogen: Rodinia breakup and development of the Pacific and Iapetus margins of Gondwana during the Neoproterozoic and Paleozoic. *Earth-Science Reviews*, **69**, 249–279, https://doi.org/10.1016/j.earscirev.2004.09.001

Chelle-Michou, C., Chiaradia, M., Ovtcharova, M., Ulianov, A. and Wotzlaw, J.-F. 2014. Zircon petrochronology reveals the temporal link between porphyry systems and the magmatic evolution of their hidden plutonic roots (the Eocene Coroccohuayco deposit, Peru). *Lithos*, **198**, 129–140, https://doi.org/10.1016/j.lithos.2014.03.017

Cherniak, D.J., Lanford, W.A. and Ryerson, F.J. 1991. Lead diffusion in apatite and zircon using ion implantation and Rutherford Backscattering techniques. *Geochimica et Cosmochimica Acta*, **55**, 1663–1673, https://doi.org/10.1016/0016-7037(91)90137-T

Chiaradia, M. 2015. Crustal thickness control on Sr/Y signatures of recent arc magmas: an Earth scale perspective. *Scientific reports*, **5**, 1–5, https://doi.org/10.1038/srep08115

Cochrane, R., Spikings, R.A. *et al.* 2014. High temperature (>350 °C) thermochronology and mechanisms of Pb loss in apatite. *Geochimica et Cosmochimica Acta*, **127**, 39–56, https://doi.org/10.1016/j.gca.2013.11.028

Cohen, K.M., Finney, S.C., Gibbard, P.L. and Fan, J.-X. 2013. The ICS international chronostratigraphic chart. *Episodes*, **36**, 199–204, https://doi.org/10.18814/epiiugs/2013/v36i3/002

Cordani, U.G. and Sato, K. 2000. Crustal evolution of the South American platform based on Nd isotopic systematics on granitoid rocks. *Episodes*, **22**, 167–173, https://doi.org/10.18814/epiiugs/1999/v22i3/003

Dalziel, I.W.D. 1981. Back-arc extension in the southern Andes: a review and critical reappraisal. *Philosophical Transactions of the Royal Society of London, Series A*, **300**, 319–335, https://doi.org/10.1098/rsta.1981.0067

Dalziel, I.W.D., de Wit, M.J. and Palmer, K.F. 1974. Fossil marginal basin in the southern Andes. *Nature*, **250**, 291–294, https://doi.org/10.1038/250291a0

Defant, M.J. and Drummond, M.S. 1990. Derivation of some modern arc magmas by melting of young subducted lithosphere. *Nature*, **347**, 662–665, https://doi.org/10.1038/347662a0

de La Roche, H., Leterrier, J., Grandclaude, P. and Marchal, M. 1980. A classification of volcanic and plutonic rocks using R1R2-diagram and major-element analyses – its relationships with current nomenclature. *Chemical Geology*, **29**, 183–210, https://doi.org/10.1016/0009-2541(80)90020-0

Ducea, M.N., Paterson, S.R. and DeCelles, P.G. 2015. High-volume magmatic events in subduction systems. *Elements*, **11**, 99–104, https://doi.org/10.2113/gselements.11.2.99

Dupre, B. and Allègre, C.J. 1980. Pb–Sr–Nd isotopic correlation and the chemistry of the North Atlantic mantle. *Nature*, **3**, 17–22, https://doi.org/10.1038/286017a0

Flowerdew, M.J., Millar, I.L., Vaughan, A.P. and Pankhurst, R.J. 2005. Age and tectonic significance of the Lassiter Coast intrusive suite, eastern Ellsworth Land, Antarctic Peninsula. *Antarctic Science*, **17**, 443–452, https://doi.org/10.1017/S0954102005002877

Flowerdew, M.J., Millar, I.L., Vaughan, A.P.M., Horstwood, M.S.A. and Fanning, C.M. 2006. The source of granitic gneisses and migmatites in the Antarctic Peninsula: a combined U–Pb SHRIMP and laser ablation Hf isotope study of complex zircons. *Contributions to Mineralogy and Petrology*, **151**, 751–768, https://doi.org/10.1007/s00410-006-0091-6

Ghidella, M.E., Yáñez, G. and LaBrecque, J.L. 2002. Revised tectonic implications for the magnetic anomalies of the western Weddell Sea. *Tectonophysics*, **347**, 65–86, https://doi.org/10.1016/S0040-1951(01)00238-4

Ghidella, M.E., Lawver, L.A. and Gahagan, L.M. 2007. *Break-up of Gondwana and Opening of the South Atlantic: Review of Existing Plate Tectonic Models*. US Geological Survey and the National Academies, **USGS OF-2007-1047**. Short Research Paper 055, https://doi.org/10.3133/ofr20071047SRP055

Gianni, G.M., Dávila, F.M. *et al.* 2018. A geodynamic model linking Cretaceous orogeny, arc migration, foreland dynamic subsidence and marine ingression in southern South America. *Earth-Science Reviews*, **185**, 437–462, https://doi.org/10.1016/j.earscirev.2018.06.016

Goodge, J.W. and Fanning, C.M. 2016. Mesoarchean and Paleoproterozoic history of the Nimrod Complex, central Transantarctic Mountains, Antarctica: Stratigraphic revisions and relation to the Mawson continent in East Gondwana. *Precambrian Research*, **285**, 242–271, https://doi.org/10.1016/j.precamres.2016.09.001

Gianni, G.M., Navarrete, C. *et al.* 2020. Northward propagation of Andean genesis: insights from Early Cretaceous synorogenic deposits in the Aysén–Río Mayo basin. *Gondwana Research*, **77**, 238–259, https://doi.org/10.1016/j.gr.2019.07.014

Grunow, A.M. 1993. Creation and destruction of Weddell Sea floor in the Jurassic. *Geology*, **21**, 647–650, https://doi.org/10.1130/0091-7613(1993)021<0647:CADOWS>2.3.CO;2

Grunow, A., Dalziel, I., Harrison, T.M. and Heizler, M.T. 1992. Structural geology and geochronology of subduction complexes along the margin of Gondwanaland: new data from the Antarctic Peninsula and southernmost Andes. *Geological Society of America Bulletin*, **104**, 1497–1514, https://doi.org/10.1130/0016-7606(1992)104<1497:SGAGOS>2.3.CO;2

Haase, K.M., Beier, C., Fretzdorff, S., Smellie, J.L. and Garbe-Schonberg, D. 2012. Magmatic evolution of the South Shetland Islands, Antarctica, and implications for continental crust formation. *Contributions to Mineralogy and Petrology*, **163**, 1103–1119, https://doi.org/10.1007/s00410-012-0719-7

Hanan, B.B. and Graham, D.W. 1996. Lead and helium isotope evidence from oceanic basalts for a common deep source of mantle plumes. *Science*, **272**, 991–995, https://doi.org/10.1126/science.272.5264.991

Hathway, B. 2000. Continental rift to back-arc basin: Jurassic–Cretaceous stratigraphical and structural evolution of the Larsen Basin, Antarctic Peninsula. *Journal of the Geological Society, London*, **157**, 417–432, https://doi.org/10.1144/jgs.157.2.417

Hervé, F., Faúndez, V., Brix, M. and Fanning, M. 2006. Jurassic sedimentation of the Miers Bluff Formation, Livingston Island, Antarctica: evidence from SHRIMP U–Pb ages of detrital and plutonic zircons. *Antarctic Science*, **18**, 229–238, https://doi.org/10.1017/S0954102006000277

Hildebrand, R.S., Whalen, J.B. and Browing, S.A. 2018. Resolving the crustal composition paradox by 3.8 billion years of slab failure magmatism and collisional recycling of continental crust. *Tectonophysics*, **734–735**, 69–88, https://doi.org/10.1016/j.tecto.2018.04.001

Hildreth, W. and Moorbath, S. 1988. Crustal contribution to arc magmatism in the Andes of central Chile. *Contributions to Mineralogy and Petrology*, **98**, 455–489, https://doi.org/10.1007/BF00372365

Homovc, J.F. and Constantini, L. 2001. Hydrocarbon exploration potential within intraplate shear-related depocenters: Deseado and San Julian basins, southern Argentina. *AAPG Bulletin*, **85**, 1795–1816, https://doi.org/10.1306/8626D077-173B-11D7-8645000102C1865D

Hunt, C.P., Banerjee, S.K., Han, J.M., Solheid, P.A., Oches, E., Sun, W.W. and Liu, T.S. 1995. Rock-magnetic proxies of climate change in the loess–palaeosol sequences of the western Loess Plateau of China. *Geophysical Journal International*, **123**, 232–244, https://doi.org/10.1111/j.1365-246X.1995.tb06672.x

Israel, L. 2015. *Geología de President Head, Isla Snow, Archipiélago del Sur, Antártica*. Geology Department, Universidad de Chile, Santiago, http://repositorio.uchile.cl/handle/2250/137605

Jokat, W., Boebel, T., König, M. and Meyer, U. 2003. Timing and geometry of early Gondwana breakup. *Journal of Geophysical Research*, **108**, https://doi.org/10.1029/2002JB001802

Jordan, T.A., Neale, R.F. *et al.* 2014. Structure and evolution of Cenozoic arc magmatism on the Antarctic Peninsula: a high resolution aeromagnetic perspective. *Geophysics Journal International*, **198**, 1758–1774, https://doi.org/10.1093/gji/ggu233

Jordan, T.A., Riley, T.R. and Siddoway, C.S. 2020. Anatomy and evolution of a complex continental margin: geologic history of West Antarctica. *Nature Reviews Earth and Environment*, **1**, 117–133, https://doi.org/10.1038/s43017-019-0013-6

Kay, S.M. and Mpodozis, C. 2001. Central Andean ore deposits linked to evolving shallow subduction systems and thickening crust. *Geological Society of America Today*, 4–9, https://doi.org/10.1130/1052-5173(2001)011<0004:CAODLT>2.0.CO;2

Kemp, A.I.S., Hawkesworth, C.J., Collins, W.J., Gray, C.M. and Blevin, P.L. 2009. Isotopic evidence for rapid continental growth in an extensional accretionary orogen: the Tasmanides, eastern Australia. *Earth and Planetary Science Letters*, **284**, 455–466, https://doi.org/10.1016/j.epsl.2009.05.011

Kirkland, C.L., Yakymchuk, C., Szilas, K., Evans, N., Hollis, J., McDonald, B. and Gardiner, N.J. 2018. Apatite: a U–Pb thermochronometer or geochronometer. *Lithos*, **318–319**, 143–157, https://doi.org/10.1016/j.lithos.2018.08.007

König, M. and Jokat, W. 2006. The Mesozoic breakup of the Weddell Sea. *Journal of Geophysical Research*, **111**, B12102, https://doi.org/10.1029/2005JB004035

Lachenbruch, A.H., Sass, J.H. and Morgan, P. 1994. Thermal regime of the southern Basin and Range Province, 2, implications of heat flow for regional extension and metamorhphic core complexes. *Journal of Geophysical Research*, **99**, 22121–22133, https://doi.org/10.1029/94JB01890

Larter, R.D. and Barker, P.F. 1991. Effects of ridge crest–trench interaction on Antarctic–Phoenix spreading: forces on a young subducting plate. *Journal of Geophysical Research*, **96**, 19583–19607, https://doi.org/10.1029/91JB02053

Leat, P.T. and Riley, T.R. 2021. Antarctic Peninsula and South Shetland Islands I. Volcanology. *Geological Society, London, Memoirs*, **55**, 185–212, https://doi.org/10/1144/M55-2018-52

Leat, P.T., Scarrow, J.H. and Millar, I.L. 1995. On the Antarctic Peninsula batholith. *Geological Magazine*, **132**, 399–4127, https://doi.org/10.1017/S0016756800021464

Leat, P.T., Flowerdew, M.J., Riley, T.R., Whitehouse, M.J., Scarrow, J.H. and Millar, I.L. 2009. Zircon U–Pb dating of Mesozoic volcanic and tectonic events in Northwest Palmer Land and Southeast Graham Land, Antarctica. *Antarctic Science*, **21**, 633–641, https://doi.org/10.1017/S0954102009990320

Maniar, P.D. and Piccoli, P.M. 1989. Tectonic discrimination of granitoids. *Geological Society of America Bulletin*, **101**, 635–643, https://doi.org/10.1130/0016-7606(1989)101<0635:TDOG>2.3.CO;2

Mantle, G.W. and Collins, W.J. 2008. Quantifying crustal thickness variations in evolving orogens: correlation between arc basalt composition and Moho depth. *Geology*, **36**, 87–90, https://doi.org/10.1130/G24095A.1

Martin, A.K. 2007. Gondwana breakup via double-saloon-door rifting and seafloor spreading in a backarc basin during subduction rollback. *Tectonophysics*, **445**, 245–272, https://doi.org/10.1016/j.tecto.2007.08.011

Martin-Gombojav, N. and Winkler, W. 2008. Recycling of Proterozoic crust in the Andean Amazon foreland of Ecuador: implications for orogenic development of the Northern Andes. *Terra Nova*, **20**, 22e31, https://doi.org/10.1111/j.1365-3121.2007.00782.x

Matthews, K.J., Seton, M. and Müller, R.D. 2012. A global-scale plate reorganization event at 105–100 Ma. *Earth and Planetary Science Letters*, **355**, 283–298, https://doi.org/10.1016/j.epsl.2012.08.023

McCarron, K. and Millar, I. 1997. The age and stratigraphy of fore-arc magmatism on Alexander Island, Antarctica. *Geological Magazine*, **134**, 507–522, https://doi.org/10.1017/S0016756897007437

Meneilly, A.W., Harrison, S.M., Piercy, B.A., and Storey, B.C. 1987. Structural evolution of the magmatic arc in northern Palmer Land, Antarctic Peninsula. *In*: Mckenzie, G.D. (ed.) *Gondwana Six: structure, tectonics, and geophysics*, **40**, 209–219, https://doi.org/10.1029/GM040p0209

Meneilly, A.W. 1988. Reverse fault step at Engel Peaks, Antarctic Peninsula. *Journal of Structural Geology*, **10**, 393–403, https://doi.org/10.1016/0191-8141(88)90017-X

Meert, J.G. and Lieberman, B.S. 2008. The Neoproterozoic assembly of Gondwana and its relationship to the Ediacaran–Cambrian radiation. *Gondwana Research*, **14**, 5–21, https://doi.org/10.1016/j.gr.2007.06.007

Millar, I.L., Pankhurst, R.J. and Fanning, C.M. 2002. Basement Chronology of the Antarctic Peninsula: recurrent magmatism and anatexis in the Palaeozoic Gondwana Margin. *Journal of the Geological Society, London*, **159**, 145–157, https://doi.org/10.1144/0016-764901-020

Morata, D. and Aguirre, L. 2003. Extensional Lower Cretaceous volcanism in the Coastal Range (29°20’–30°S), Chile: geochemistry and petrogenesis. *Journal of South American Earth Sciences*, **16**, 459–476, https://doi.org/10.1016/j.jsames.2003.06.001

Mpodozis, C. and Allmendinger, R.W. 1993. Extensional tectonics, Cretaceous Andes, northern Chile (27°S). *Geological Society of America Bulletin*, **105**, 1462–1477, https://doi.org/10.1130/0016-7606(1993)105<1462:ETCANC>2.3.CO;2

Mpodozis, C. and Ramos, V.A. 1989. The Andes of Chile and Argentina. *Circum-Pacific Council for Energy and Mineral Resources Earth Sciences Series*, **11**, 59–90.

Mpodozis, C., Arriagada, C., Basso, M., Roperch, P., Cobbold, P. and Reich, M. 2005. Late Mesozoic to Paleogene stratigraphy of the Salar de Atacama Basin, Antofagasta, Northern Chile: implications for the tectonic evolution of the Central Andes. *Tectonophysics*, **399**, 125–154, https://doi.org/10.1016/j.tecto.2004.12.019

Nelson, D.A. and Cottle, J.M. 2017. Long-term geochemical and geodynamic segmentation of the paleo-Pacific margin of Gondwana: insight from the Antarctic and adjacent sectors. *Tectonics*, **36**, 3229–3247, https://doi.org/10.1002/2017TC004611

Nelson, D.A. and Cottle, J.M. 2018. The secular development of accretionary orogens: linking the Gondwana magmatic arc record of West Antarctica, Australia and South America. *Gondwana Research*, **63**, 15–33, https://doi.org/10.1016/j.gr.2018.06.002

Oliveros, V., Vasquez, P. *et al.* 2019. Lithospheric evolution of the Pre- and Early Andean convergent margin, Chile. *Gondwana Research*, **80**, 202–227, https://doi.org/10.1016/j.gr.2019.11.002

Pankhurst, R.J. 1982. Rb–Sr geochronology of Graham Land. *Journal of the Geological Society, London*, **139**, 701–711, https://doi.org/10.1144/gsjgs.139.6.0701

Pankhurst, R.J. 1983. Rb–Sr constraints on the ages of basement rocks of the Antarctic Peninsula. *In:* Oliver, R.L., James, P.R. and Jago, J.B. (eds) *Antarctic Earth Science*. Australian Academy of Science, Canberra, ACT, 367–371.

Pankhurst, R.J. 1990. The Paleozoic and Andean magmatic arcs of West Antarctica and southern South America. *Geological Society of America, Special Papers*, **241**, 1–7.

Pankhurst, R.J., Rowley, P.D., Thomson, M.R.A., Crame, J.A. and Thomson, J.W. 1991. Rb-Sr study of Cretaceous plutons from southern Antarctic Peninsula and eastern Ellsworth Land, Antarctica. *Geological evolution of Antarctica*, **1**, 387.

Pankhurst, R.J., Riley, T.R., Fanning, C.M. and Kelley, S.P. 2000. Episodic silicic volcanism in Patagonia and the Antarctic Peninsula: chronology of magmatism associated with the breakup of Gondwana. *Journal of Petrology*, **41**, 603–625, https://doi.org/10.1093/petrology/41.5.605

Paterson, S.R. and Ducea, M.N. 2015. Arc magmatic tempos: Gathering the evidence. *Elements*, **11**, 91–98, https://doi.org/10.2113/gselements.11.2.91

Peacock, M.A. 1931. Classification of igneous rock series. *Journal of Geology*, **39**, 54–67, https://doi.org/10.1086/623788

Pearce, J.A., Harris, N.B.W. and Tindle, A.G. 1984. Trace element discrimination diagrams for the tectonic interpretation of granitic rocks. *Journal of Petrology*, **25**, 956–983, https://doi.org/10.1093/petrology/25.4.956

Petrus, J.A. and Kamber, B.S. 2012. VizualAge: A novel approach to laser ablation ICP-MS U-Pb geochronology data reduction. *Geostandards and Geoanalytical Research*, **36**, 247–270, https://doi.org/10.1111/j.1751-908X.2012.00158.x

Poblete, F., Arriagada, C., Roperch, P., Astudillo, N., Herve, F., Kraus, S. and Le Roux, J.P. 2011. Paleomagnetism and tectonics of the South Shetland Islands and the northern Antarctic Peninsula. *Earth and Planetary Science Letters*, **302**, 299–313, https://doi.org/10.1016/j.epsl.2010.12.019

Profeta, L., Ducea, M.N. *et al.* 2015. Quantifying crustal thickness over time in magmatic arcs. *Scientific Reports*, **5**, 17786, https://doi.org/10.1038/srep17786

Riley, T.R., Leat, P.T., Pankhurst, R.J. and Harris, C. 2001. Origins of large volume rhyolitic volcanism in the Antarctic Peninsula and Patagonia by crustal melting. *Journal of Petrology*, **42**, 1043–1065, https://doi.org/10.1093/petrology/42.6.1043

Riley, T.R., Flowerdew, M.J. and Whitehouse, M.J. 2012. Chrono- and lithostratigraphy of a Mesozoic–Tertiary fore- to intra-arc basin: Adelaide Island, Antarctic Peninsula. *Geological Magazine*, **149**, 768–782, https://doi.org/10.1017/S0016756811001002

Riley, T.R., Curtis, M.L., Flowerdew, M.J. and Whitehouse, M.J. 2016. Evolution of the Antarctic Peninsula lithosphere: evidence from Mesozoic mafic rocks. *Lithos*, **244**, 59–73, https://doi.org/10.1016/j.lithos.2015.11.037

Riley, T.R., Flowerdew, M.J., Pankhurst, R.J., Curtis, M.L., Millar, I.L., Fanning, C.M. and Whitehouse, M.J. 2017. Early Jurassic magmatism on the Antarctic Peninsula and potential correlation with the Subcordilleran plutonic belt of Patagonia. *Journal of the Geological Society, London*, **174**, 365–376, https://doi.org/10.1144/jgs2016-053

Riley, T.R., Burton-Johnson, A., Flowerdew, M.J. and Whitehouse, M.J. 2018. Episodicity within a mid-Cretaceous magmatic flare-up in West Antarctica: U–Pb ages of the Lassiter Coast intrusive suite, Antarctic Peninsula, and correlations along the Gondwana margin. *Geological Society of America Bulletin*, **130**, 1177–1196, https://doi.org/10.1130/B31800.1

Riley, T., Flowerdew, M., Burton-Johnson, A., Leat, P., Millar, I. and Whitehouse, M. 2020*a*. Cretaceous arc volcanism of Palmer Land, Antarctic Peninsula: Zircon U–Pb geochronology, geochemistry, distribution and field relationships. *Journal of Volcanology and Geothermal Research*, **401**, 106969, https://doi.org/10.1016/j.jvolgeores.2020.106969

Riley, T.R., Jordan, T.A., Leat, P.T., Curtis, M.L. and Millar, I.L. 2020*b*. Magmatism of the Weddell Sea rift system in Antarctica: implications for the age and mechanism of rifting and early stage Gondwana breakup. *Gondwana Research*, **79**, 185–196, https://doi.org/10.1016/j.gr.2019.09.014

Rowley, P.D., Vennum, W.R., Kellogg, K.S., Laudon, T.S., Carrara, P.E., Boyles, J.M. and Thomson, M.R.A. 1983. Geology and plate tectonic setting of the Orville Coast and eastern Ellsworth Land. Antarctica. *In:* Oliver, R.L., James, P.R. and Jago, J.B. (eds) *Antarctic Earth Science*. Australian Academy of Science, Canberra, ACT, 245–250.

Ryan, C. 2007. *Mesozoic to Cenozoic Igneous Rocks from Northwestern Graham Land: Constraints on the Tectonomagmatic Evolution of the Antarctic Peninsula*. PhD thesis, University of Brighton.

Sarmiento, L.F. and Rangel, A. 2004. Petroleum systems of the Upper Magdalena Valley, Colombia. *Marine and Petroleum Geology*, **21**, 373–391, https://doi.org/10.1016/j.marpetgeo.2003.11.019

Spikings, R., Cochrane, R., Villagomez, D., Van der Lelij, R., Vallejo, C., Winkler, W. and Beate, B. 2015. The geological history of northwestern South America: from Pangaea to the early collision of the Caribbean Large Igneous Province (290–75 Ma). *Gondwana Research*, **27**, 95–139, https://doi.org/10.1016/j.gr.2014.06.004

Spikings, R., Rietsma, M. *et al.* 2016. Characterisation of Triassic rifting in Peru and implications for the early disassembly of western Pangaea. *Gondwana Research*, **35**, 124–143, https://doi.org/10.1016/j.gr.2016.02.008

Stern, R.J. 2002. Subduction zones. *Reviews of Geophysics*, **40**, 1012, https://doi.org/10.1029/2001RG000108

Storey, B.C., Brown, R.W., Carter, A., Doubleday, P.A., Hurford, A.J., Macdonald, D.I.M. and Nell, P.A.R. 1996. Fission-track evidence for the thermotectonic evolution of a Mesozoic–Cenozoic fore-arc, Antarctica. *Journal of the Geological Society, London*, **153**, 65–82, https://doi.org/10.1144/gsjgs.153.1.0065

Stracke, A., Bizimis, M. and Salters, V.J.M. 2003. Recycling oceanic crust: quantitative constraints. *Geochemistry, Geophysics, Geosystems*, **4**, 8003, https://doi.org/10.1029/2001GC000201

Suárez, M. 1976. Plate-tectonic model for southern Antarctic Peninsula and its relation to southern Andes. *Geology*, **4**, 211–214, https://doi.org/10.1130/0091-7613(1976)4<211:PMFSAP>2.0.CO;2

Sun, S.S. and McDonough, W.F. 1989. Chemical and isotopic systematics of oceanic basalts: implications for mantle composition and processes. *Geological Society, London, Special Publications*, **42**, 313–345, https://doi.org/10.1144/GSL.SP.1989.042.01.19

Sutherland, R. and Hollis, C. 2001. Cretaceous demise of the Moa plate and strike–slip motion at the Gondwana margin. *Geology*, **29**, 279–282, https://doi.org/10.1130/0091-7613(2001)029<0279:CDOTMP>2.0.CO;2

Taylor, S.R. and McLennan, S.M. 1995. The geochemical evolution of the continental crust. *Reviews of Geophysics*, **33**, 241–265, https://doi.org/10.1029/95RG00262

Thomson, M.R.A. and Pankhurst, R.J. 1983. Age of Post-Gondwanian calcalkaline volcanism in the Antarctic Peninsula region. *In:* Oliver, R.L., James, P.R. and Jago, J.B. (eds) *Antarctic Earth Science*. Australian Academy of Science, Canberra, ACT, 328–333.

Vaughan, A.P.M. 1995. Circum-Pacific mid-Cretaceous deformation and uplift: a superplume-related event? *Geology*, **23**, 491–494, https://doi.org/10.1130/0091-7613(1995)023<0491:CPMCDA>2.3.CO;2

Vaughan, A.P.M. and Livermore, R.A. 2005. Episodicity of Mesozoic terrane accretion along the Pacific margin of Gondwana: implications for superplume–plate interactions. *Geological Society, London, Special Publications*, **246**, 143–178, https://doi.org/10.1144/GSL.SP.2005.246.01.05

Vaughan, A.P.M. and Pankhurst, R.J. 2008. Tectonic overview of the West Gondwana margin. *Gondwana Research*, **13**, 150–162, https://doi.org/10.1016/j.gr.2007.07.004

Vaughan, A.P.M. and Storey, B.C. 2000. The eastern Palmer Land shear zone: a new terrane accretion model for the Mesozoic development of the Antarctic Peninsula. *Journal of the Geological Society, London*, **157**, 1243–1256, https://doi.org/10.1144/jgs.157.6.1243

Vaughan, A.P.M., Wareham, C.D., Johnson, A.C. and Kelley, S.P. 1998. A Lower Cretaceous, syn-extensional magmatic source for a linear belt of positive magnetic anomalies: the Pacific Margin Anomaly (PMA), western Palmer Land, Antarctica. *Earth and Planetary Science Letters*, **158**, 143–155, https://doi.org/10.1016/S0012-821X(98)00054-5

Vaughan, A., Kelley, S. and Storey, B. 2002*a*. Mid-Cretaceous ductile deformation on the Eastern Palmer Land Shear Zone, Antarctica, and implications for timing of Mesozoic terrane collision. *Geological Magazine*, **139**, 465–471, https://doi.org/10.1017/S0016756802006672

Vaughan, A.P.M., Pankhurst, R.J. and Fanning, C.M. 2002*b*. A mid-Cretaceous age for the Palmer Land event, Antarctic Peninsula: implications for terrane accretion timing and Gondwana palaeolatitudes. *Journal of the Geological Society, London*, **159**, 113–116, https://doi.org/10.1144/0016-764901-090

Vaughan, A.P.M., Leat, P.T., Dean, A.A. and Millar, I.L. 2012. Crustal thickening along the West Antarctic Gondwana margin during mid-Cretaceous deformation of the Triassic intra-oceanic Dyer Arc. *Lithos*, **142–143**, 130–147, https://doi.org/10.1016/j.lithos.2012.03.008

Villagómez, D. and Spikings, R. 2013. Thermochronology and tectonics of the Central and Western Cordilleras of Colombia: early Cretaceous–Tertiary evolution of the Northern Andes. *Lithos*, **168**, 228–249, https://doi.org/10.1016/j.lithos.2012.12.008

Wever, H.E., Millar, I.L. and Pankhurst, R.J. 1994. Geochronology and radiogenic isotope geology of Mesozoic rocks from eastern Palmer Land, Antarctic Peninsula: crustal anatexis in arc-related granitoid genesis. *Journal of South American Earth Sciences*, **7**, 69–83, https://doi.org/10.1016/0895-9811(94)90035-3

Whalen, J.B. and Hildebrand, R.S. 2019. Trace element discrimination of arc, slab failure, and A-type granitic rocks. *Lithos*, **348–349**, 105179, https://doi.org/10.1016/j.lithos.2019.105179

Zartman, R.E. and Doe, B.R. 1981. Plumbotectonics – the model. *Tectonophysics*, **75**, 135–162, https://doi.org/10.1016/0040-1951(81)90213-4

Zheng, G.G., Liu, X., Liu, S., Zhang, S.H. and Zhao, Y. 2018. Late Mesozoic–early Cenozoic intermediate–acid intrusive rocks from the Gerlache Strait area, Antarctic Peninsula: zircon U–Pb geochronology, petrogenesis and tectonic implications. *Lithos*, **312–313**, 204–222, https://doi.org/10.1016/j.lithos.2018.05.008